Chapter 2

Fabrication and Characterization of Silk Fibroin- Soy Protein based Nanofibrous Scaffolds for Skin Tissue Engineering

2.1 Introduction

TE of biological skin substitutes has significantly progressed over a period to deliver a promising solution for the treatment of skin injuries such as closing and healing of acute and chronic wounds. In the literature, various biomaterials have been used for wound dressing material including natural and synthetic polymers (H. Chen et al. 2011; Mogoşanu and Grumezescu 2014). The protein-based biomaterials are the potential scaffolds useful for various applications, including TE, controlled drug delivery systems, filtration and food industry applications (Jao et al. 2017; Tansaz et al. 2017; DeFrates et al. 2018; Nagarajan et al. 2017). They provide similar molecular structures and biological functionality as natural proteins in tissue. Several research efforts have been made and reported in the literature on the utilization of different protein based scaffolds for diverse TE applications. In particular, Olami et al. have fabricated a drug-loaded, SPI based scaffold for skin tissue regeneration (Olami, Berdicevsky, and Zilberman 2015). In another work, Nagaranjan et al. have designed a gelatin based electrospun nanofibers for bone TE (Nagarajan et al. 2017). A collagen based shape-memory scaffold for cartilage regeneration has been developed by Jiang et al. (Jiang et al. 2018). The present study relates to the development of nanofibrous scaffolds using novel protein blends viz., SPI and SF for skin TE applications.

SPI is a globular protein that has various advantages over other natural biomaterials such as biocompatibility, non-immunogenicity, high availability, non-toxicity, biodegradability, low price, long-time stability and storage (Y. Wang, Cao, and Zhang 2006; Li, Peshkova, and Geng 2004; Chien et al. 2013; G. A. Silva et al. 2003). The presence of multiple functional groups such as -OH, -SH, -NH_2 and –COOH render it an accessible choice for physical and chemical modifications (Khatib et al. 2002; Ramji and Shah 2014). The proposed plant-derived polymer can efficiently replace the animal origin

proteins, thereby decreasing the risk of infection due to transmissible disease and does not raise any ethical and cultural issues. Therefore, it can be a good and safe alternative for animal origin proteins to mimic the human ECM, aiding in blood clot formation and tissue regeneration. It also helps in modulating cell migration, adhesion, and proliferation because of the presence of cell adhesive moieties. In particular, the soybean-based biomaterial can offer a solution to many challenges experienced during the regeneration of broken bones and damaged tissues (Merolli et al. 2010; Santin et al. 2007). In addition, it has been reported that these materials have a significant potential towards wound healing through stimulating the cells for tissue regeneration, collagen deposition and their integration into a blood clot. The use of these materials eliminates the need of additional growth factors (Santin and Ambrosio 2008). Antibiotics containing biodegradable soy protein membranes have also been prepared for wound dressing applications (Peles and Zilberman 2012).

SF possesses many interesting properties desired for biomedical applications such as biocompatibility, low immunogenicity, adequate permeability to oxygen and water vapor, non-toxicity, low cost and robust mechanical properties (Dadras Chomachayi et al. 2018; Marelli et al. 2012). However, its use in TE is limited because of its very slow mass loss rate. Therefore, several studies have been conducted to improve the properties of SF such as degradation, cell attachment, etc. by blending it with other polymers, for example, chitin (Park et al. 2006), elastin (Vasconcelos, Gomes, and Cavaco-Paulo 2012), gelatin (Yin-Guibo et al. 2009) and poly(lactide-co-glycolic acid) (PLGA) (Shahverdi et al. 2014).

A number of methods have been developed to fabricate scaffolds for skin TE applications such as freeze drying, freeze-thaw, 3-D printing, salt leaching, electrospinning, phase

separation, etc (Nicholas, Jeschke, and Amini-Nik 2016; Eltom, Zhong, and Muhammad 2019; Varshney et al. 2019; Lu, Li, and Chen 2013). Among them, in this chapter, electrospinning technique has been employed for nanofibrous structure formation. The nanofibrous structure provides a large surface to volume ratio and high porosity that together offers enough space for drug loading, cell incorporation, migration and proliferation (Ye et al. 2019). Electrospinning based scaffold fabrication is a promising approach for various TE applications such as wound dressing, drug delivery, artificial skin substitute, microengineered platform etc. (Thenmozhi et al. 2017; Bhardwaj and Kundu 2010b). In addition, it has found applications in diverse areas such as nanosensors, cosmetics, separation, filtration membrane, water treatment and purifications, environmental remediation, and smart textiles (Barhoum et al. 2019). SPI cannot be electrospun alone due to its low molecular weight; therefore, it is mixed with either a synthetic or natural polymer. Some research groups have explored SPI-blends with other polymers including PVA, chitosan, polyacrylonitrile (PAN), polyethylene oxide (PEO), PLA, PCL and zein etc. (Salas et al. 2014; Xu et al. 2012; Thirugnanaselvam, Gobi, and Arun Karthick 2013; Cho, Netravali, and Joo 2012). Hence, we have tested a hypothesis that SPI/SF protein blends could be potentially useful to develop functionally improved and mechanically stable nanofibrous scaffolds using the electrospinning approach, in particular, for the recreation of tissue constructs.

In this chapter, we present the fabrication and functional characterization of electrospun nanofibers using the novel protein blends. To the best of our knowledge, we present for the first time the electrospinning of SPI and SF blend. These polymers were mixed in an appropriate ratio in formic acid to obtain a viscous solution suitable for electrospinning. The blend so formed can be used for extruding fibers through electrospinning. The ratio of the amount of SPI and SF altogether decides the rate of extrusion and fiber formation

through a syringe needle under electrostatic force. The developed protein mixture exhibits excellent fiber formation capability, which is otherwise difficult with SPI alone. The blend nanofibrous sheet can serve as a potential platform for TE that could be used for both in vitro and in vivo applications. The fabricated electrospun nanofibers were morphologically analyzed by the SEM micrographs. Porosity was also measured from SEM micrographs through the image analysis method. The prepared scaffolds were treated with ethanol vapors (EtOH) to convert the random coils into β sheets in SF and bring stability into the structure. The intermolecular interactions were evaluated by attenuated total reflectance-Fourier transform infrared (ATR-FTIR) spectroscopy. The thermal stability of scaffolds was examined by thermogravimetric analysis (TGA). The water holding capacity and stability of scaffolds were studied in phosphate buffered saline (PBS) at a room temperature and as well as at 37˚C (i.e., physiological temperature). In vitro degradation was assessed in a lysozyme-containing solution for up to 20 days at 37˚C. In vitro cytotoxicity and the extent of proliferation of fibroblast and melanocyte cells were studied using the fabricated nanofibrous scaffolds. Furthermore, we also examined the biocompatibility of prepared nanofibrous scaffolds using a rat model for full-thickness wound healing.

2.2 Materials and methods

2.2.1 Materials

SPI powder was procured from A.M. NUTRATECH Pvt. Ltd., India. Cocoons of Bombyx mori silkworm were purchased from Research Extension (Silk Board), Bhadrasi, Varanasi, Ministry of Textiles, Government of India. Dialysis membrane [12,000 molecular weight cut off (MWCO)], polyethylene glycol (PEG, molecular weight - 20,000) (25322-68-3), lithium bromide (LiBr) (7550-35-8), PBS (TS1101), trypsin (0.25%)–EDTA (0.038%) (TCL048), Dulbecco's modified Eagle medium (DMEM) high

glucose (AL007A), fetal bovine serum (FBS) (RM9955), antibiotics penicillin and streptomycin solution (A001), trypan blue (TC193), 4% paraformaldehyde (TC119), triton X-100 (MB031), MTT (3-[4,5-dimethyl-thiazol-2-yl]- 2,5-diphenyltetrazolium bromide) assay kit (TC151), 4,6-diamidino-2- phenylindole (DAPI) (TC229) and dimethyl sulfoxide (DMSO) (TC185) were procured from HiMedia, India. Formic acid (98%) of LOBA CHEMIE Pvt. Ltd. was used. Petri dish 35 mm (460035, TARSON), centrifuge tube- 15 and 50 mL (GENETIX) and 96 well plate (30096, GENETIX) were used in this work. Absolute ethanol of 99.9% high analytical grade and pure distilled water was used in all the experiments.

2.2.2 Preparation of dry silk fibroin film

Firstly, cocoons were boiled in a 0.02 M Na_2CO_3 aqueous solution for 45 min, followed by washing with distilled water to clear away sericin protein from fibroin. The degummed SF was allowed to dry in a fume hood overnight. The dried fibers were dissolved into the lithium bromide solution in an oven at 60˚C for 4 h. The obtained solution was dialyzed by means of a dialysis membrane in distilled water for 48 h under continuous stirring at 300 rpm. During dialysis, water was changed several times to make a salt gradient (Rockwood et al. 2011). Moreover, the obtained SF solution was poured into a dish and kept for drying in a hot air oven at 50˚C overnight to obtain a silk film (Figure 2.1).

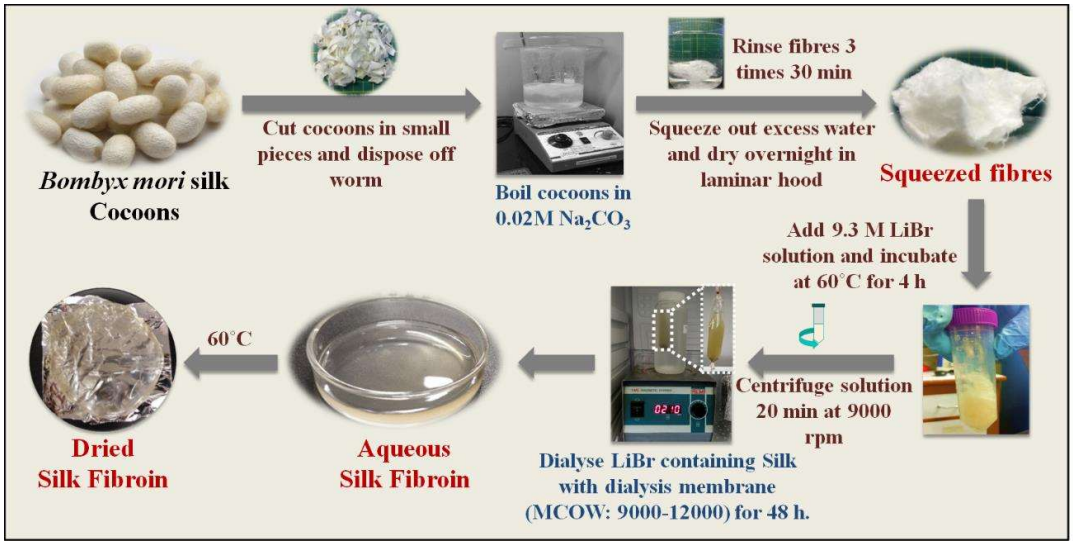

Figure 2.1 Schematic representation of procedure of silk fibroin extraction from *Bombyx mori* silk Cocoons.

2.2.3 Preparation of protein blend solution for electrospinning

In this study, the total polymer concentration for all the samples was fixed at 10% w/v. The blend mixture was prepared in five different ratios namely: 100% SPI (w/w), 75% SPI+ 25% SF (w/w), 50% SPI+ 50% SF (w/w), 25% SPI+ 75% SF (w/w) and 100 % SF (w/w) in formic acid (listed in Table 2.1). Firstly, we mixed the SPI powder to 98% formic acid for an hour at 60˚C followed by the addition of a dried SF film. The solution was continuously mixed on a magnetic stirrer for the next 11 h at room temperature. The solution was then cautiously filled into a syringe avoiding any air gaps or bubbles. The electrospinning of polymeric solution was done at room temperature (Figure 2.2). The optimized parameters of the electrospinning process are provided in Table 2.2. The obtained nanofibrous mats were dried overnight at room temperature. The dried nanofibers were then treated with 70% (v/v) aqueous ethanol vapors in a vacuum desiccator for 12 h.

Table 2.1 Formulations of spinning solutions containing SPI and SF in formic acid.

Sample (10% w/v)	SPI (g)	SF (g)	Formic acid (mL)
100 SPI	1.00	0	10
75/25 SPI/SF	0.75	0.25	10
50/50 SPI/SF	0.50	0.50	10
25/75 SPI/SF	0.25	0.75	10
100 SF	0	1.00	10

Table 2.2 Optimized values of electrospinning parameters for the prepared formulations.

Parameters	Optimized values
Flow rate	0.4 mL/h
Applied high voltage	15-18 kV
Distance between the needle and collector	13 cm
Collector type	Rotating drum collector
Needle Size	22-gauge bevel tip needle
Syringe inner diameter	16 mm
Syringe volume	10 mL

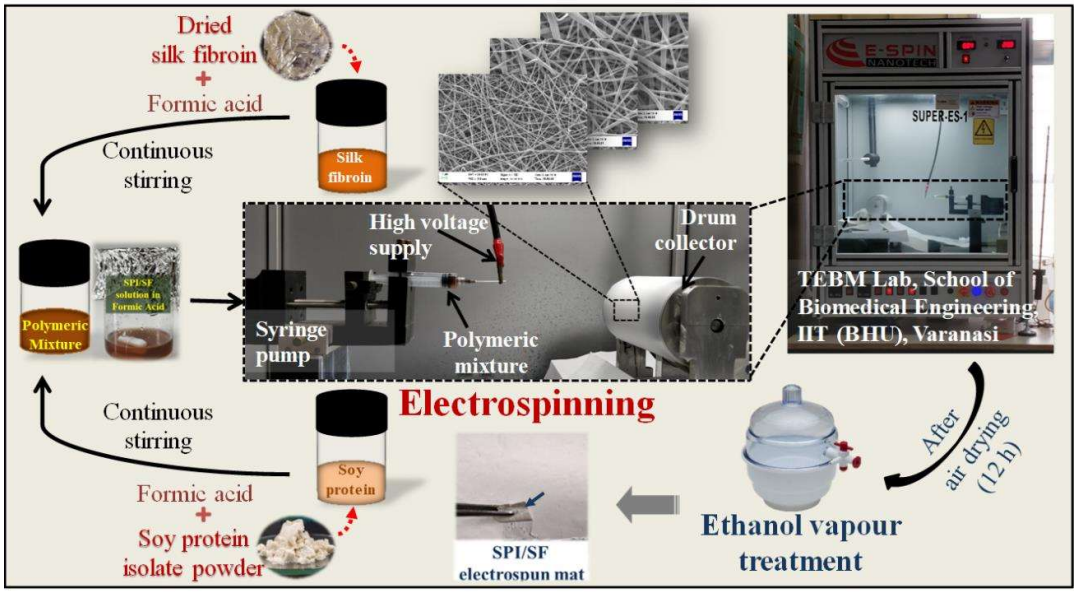

Figure 2.2 Schematic representation of SPI/SF electrospun mat fabrication process using electrospinning technique.

2.2.4 Characterization of the scaffolds

2.2.4.1 SEM analysis

The morphological characterization and fiber diameter distribution of the electrospun mats were determined with the help of SEM. The prepared samples were cut into very small pieces and then coated with gold for SEM imaging using a Zeiss EVO 18 SEM Zeiss, Oberkochen, Germany at 20 kV. The photomicrographs so obtained were further used for fiber diameter analysis, fiber orientation, and calculation of porosity percentage using ImageJ software.

The diameter of the fibers was manually measured through ImageJ software (NIH, USA) using at least five different images of each sample. Moreover, porosity was also measured using the same software from at least five different SEM images of each sample. Porosity measurement by image analysis through ImageJ software delivers 95% reliability level. For porosity calculation, all the images were first converted into binary images using

thresholding. Subsequently, the porosity was calculated using the steps enumerated as follows: 1) open image, 2) set scale bar, 3) crop desired section of image for analysis, 4) adjust threshold, and 5) analyze particles.

2.2.4.2 ATR-FTIR spectroscopic analysis

Infrared spectra for the scaffolds were recorded on ALPHA BRUKER Eco-ATR equipped with ZnSe ATR accessory. All spectra were taken at an infrared range of 500–4000 cm^{-1} and 4 cm^{-1} resolution with 24 scans. The presence of respective functional groups in the scaffolds before and after EtOH vapor treatment was analyzed through ATR-FTIR spectroscopy.

2.2.4.3 Swelling capacity

The swelling capacity of the scaffolds was measured by immersing the scaffolds in PBS solution of pH 7.4 at room temperature for 48 h. At regular intervals of time, the samples were removed from the solution and weighed using the precision electronic weighing balance after blotting the excess water by tissue paper. The samples were tested in triplicates. The swelling percentage was determined as

$$\text{Swelling } (\%) = \left(\frac{W_{wet} - W_{dry}}{W_{dry}}\right) \times 100, \tag{2.1}$$

where W_{dry} and W_{wet} are the weights of the sample before and after immersion into PBS solution, respectively.

2.2.4.4 Stability and degradation

The stability and degradation of the fabricated fibrous scaffolds were examined by soaking the samples in PBS solution (pH 7.4) and lysozyme-containing solution (10^4 U/mL in distilled water) at room temperature as well as at 37˚C. The lysozyme

degradation was observed up to 20 days, while the solution was changed after every three days. Samples were removed from the solution at a predetermined time i.e., 10^{th} and 20^{th} day followed by twice washing with distilled water. The weight loss percentage was calculated using the following formula-

$$Weight\ loss\ (\%) = \left(\frac{W_i - W_f}{W_i}\right) \times 100, \quad \textbf{(2.2)}$$

where W_i and W_f are the initial and final weights of the samples respectively, that is before and after degradation.

2.2.4.5 Transparency percentage

Transparency of the nanofibrous scaffolds was measured through a UV-visible spectrophotometer (UV-VIS Spectrophotometer – 2373, Electronics India (EI), India) at the range of visible wavelengths (400-700 nm). The samples were cut into a rectangular shape of dimensions 20 mm x 9 mm with a thickness range of approximately 0.2 to 0.3 mm. For measuring transparency, the wet scaffolds were loaded in a cuvette filled with PBS solution. The cuvette containing PBS was set as a reference baseline, and then the samples were scanned in the visible range of 400-700 nm wavelength.

2.2.4.6 Thermal stability

The thermal degradation of nanofibrous scaffolds was examined by TGA-50 thermogravimetric analyzer (Shimadzu (Asia Pacific) Pte Ltd.). TGA determines the weight or mass transition with respect to the atmosphere, time, and temperature. The study was performed in the temperature range 20˚C - 500˚C with a heating rate of 20˚C/min in nitrogen.

2.2.4.7 Cytocompatibility study

2.2.4.7.1 Fluorescent microscopic analysis

In this work, we utilized NIH-3T3 (fibroblast), L929-RFP (fibroblast) and B16-F10 (melanoma) cells. Cells were maintained in a complete nutrient medium containing DMEM, 10% FBS and 1% penicillin (10.000 U/mL)/streptomycin (10 mg/mL) in a CO_2 incubator (Galaxy® 170 S, Eppendorf, Germany) at 37˚C, 5% CO_2 and 95% relative humidity. The prepared nanofibrous scaffolds were first cut into 10 mm circular discs. They were then dipped into a complete DMEM medium in a 35 mm non-culture grade sterile Petri dish. After some time, the media was removed and each of the scaffold was seeded with 10^4 cells. The scaffolds were then incubated for the adherence of the cells on the nanofibrous scaffolds. After an hour, the Petri dishes were filled with 2 mL of complete nutrient medium and incubated in a CO_2 incubator. The culture medium was changed every alternate day. For imaging, the cells-laden scaffolds were shifted to new Petri dishes to avoid the interference from cells that had migrated and adhered to the surface of the Petri dish during incubation.

For fluorescent microscopic cell culture studies, we utilized specifically L929-RFP (red fluorescent protein) and B16-F10 cell lines, which are fibroblast and melanocyte cells, respectively. L929-RFP cells are genetically engineered fluorescent cells that were helpful in locating and visualizing the cells within the scaffolds in situ (Varshney et al. 2019; Poddar et al. 2019). These genetically engineered cells emit red fluorescence when exposed to green light under a fluorescence microscope. This facilitates the identification and evaluation of cell proliferation within a scaffold with ease. L929-RFP seeded scaffolds were directly observed under the fluorescent microscope without staining with

any dye. Whereas, B16-F10 cells loaded in the scaffolds were observed under the fluorescent microscope using a staining dye.

2.2.4.7.2 Nuclear staining

For visualization of B16-F10 cells within the scaffold, the nuclei were stained with fluorescent stain DAPI (1 μg/mL), which binds with A-T rich region in DNA. The culture medium was discarded from the sample and washed three times with PBS followed by fixation through 4% paraformaldehyde. The samples were washed after 15 min of fixation and incubated with 0.1% (v/v) Triton X-100 for 5 min. 1% bovine serum albumin (BSA) solution was then added to block the nonspecific binding of stain. Unbound BSA was washed with PBS, followed by 30 min incubation of DAPI (1 μg/mL) in a dark room (Varshney et al. 2019; Bandyopadhyay et al. 2018). Finally, samples were observed under a fluorescent microscope.

2.2.4.7.3 MTT assay

To determine the cellular proliferation, we performed MTT reduction assay. For this purpose, we used NIH-3T3 and B16-F10 cell lines. Since, for MTT assay fluorescent cells are not preferable, we have chosen wild type of fibroblast cells, i.e. NIH-3T3 cells instead of L929-RFP cells. The assay was carried out on a 4 mm diameter circular nanofibrous scaffold disc placed in the 96-well plate using the standard assay procedure. The scaffolds were sterilized by 30 min exposure of ultra-violet radiation in a biosafety cabinet. Cells were seeded at a density of 1×10^4 cells per scaffold and incubated in a CO_2 incubator for 2 and 4 days. For all the experiments, cells cultured without scaffold in wells were taken as a positive control, whereas complete nutrient medium alone was considered as a negative control for all the experiments. After incubation, the scaffolds were transferred into a new well to avoid the chances of getting false reading because of the cells which had migrated and adhered to the surface of the well during the incubation period.

Thereafter, we added a total volume of 100 µL solution containing 90 µL complete growth medium and 10 µL MTT solution (5 mg/mL in PBS) in each well and allowed to incubate for 4 h. After incubation, formed formazan crystals in each well were solubilized with 100µL dimethyl sulfoxide (DMSO) for 15 min (Poddar et al. 2019). After gentle mixing, the solution mixture was shifted to a fresh well. The optical absorbance readings were taken in a multimode reader (Synergy H1 hybrid, Biotek, USA) at a wavelength of 570 nm. All the experiments were performed in triplicates for each cell line.

2.2.4.7.4 Morphological observations of cells

For cell attachment and morphological evaluation, the cells loaded in the prepared nanofibrous scaffolds were examined through SEM. NIH-3T3 cells were seeded on the nanofibrous scaffolds at a density of 1×10^5 cells per scaffold using the process similar to the one described above. After 48 h, these scaffolds were fixed using 4% paraformaldehyde for 30 min followed by PBS washing. Subsequently, the samples were dehydrated using different concentrations of ethanol i.e. 20%, 40%, 60%, 80%, 90% and 100%. Finally, samples were dried in air and coated with gold to observe using SEM imaging.

2.2.4.8 In vivo wound healing study

The prepared nanofibrous scaffolds were examined for wound healing in healthy adult Wistar rats through circular wound excision. All the experiments were performed only after the approval of the Central Animal Ethical Committee (CAEC) of Banaras Hindu University, Varanasi (No. Dean/2018/CAEC/804). Total six rats (male, age: 5-7 months) of weights 150-250 g were used in the experiment. For anesthetizing, an intraperitoneal injection of a combination of ketamine (35 mg/kg) and xylazine (5-10 mg/kg) was given. Hair from the dorsal side were shaved off and the skin underneath was wiped with 70%

ethanol. A full-thickness circular wound was created by excision of approximately 10 mm diameter skin. The animals were divided into two groups, each containing three rats (n = 3): Group A (50/50 SPI/SF (T)), Group B (sham). Images of the wound were captured at regular intervals using a digital camera and the wound area was traced on a transparent sheet. The traced area was then calculated from the graph paper. Wound closure area progression was determined as

$$Wound\ closure\ (\%) = \left(\frac{A_i - A_d}{A_i}\right) \times 100, \quad \textbf{(2.3)}$$

where A_i and A_d denote the area of the wound on day 0 and different days post wounding, respectively. After 14 days, treated skin was excised from the rat and fixed with 4% formalin, followed by serial dehydration steps. Small sections of dehydrated skin tissue were permeated with liquid paraffin and embedded in paraffin to make tissue blocks. These tissue blocks were then sectioned by a microtome followed by hematoxylin and eosin (H&E) staining. Slides were visualized under an upright bright-field microscope (OLYMPUS, India) and images were captured using ToupView 3.7 software.

2.2.5 Statistical analysis

All the above experiments were performed in triplicates and the results were expressed as mean ± standard deviation (SD). For all the samples, a one-way analysis of variance (ANOVA) was performed for the statistical analysis with Tukey's multiple comparison tests. Two sets of data were considered statistically different when $p < 0.05$. All graphs were prepared using OriginPro 2020 (OriginLab, Learning edition). Background noise was removed from fluorescent images through ImageJ software. The Gaussian blur function was applied to individually convolve the image followed by subtraction from respective raw fluorescent images to avoid the background noise.

2.3 Results

2.3.1 SEM analysis of the fabricated electrospun mats

The electrospun blend mixtures of SPI and SF proteins were prepared in formic acid solvent in five different combinations i.e. 100 SPI, 75/25 SPI/SF, 50/50 SPI/SF, 25/75 SPI/SF and 100 SF. Ethanol treated (T) as well as non-treated electrospun (NT) scaffolds were analyzed through SEM images (Figure 2.4). Formation of the nanofibers was not observed when 100 % SPI (100 SPI) was electrospun, inferring that it is not possible to fabricate the pure SPI nanofibers in the given conditions (Figure 2.3). On the other hand, the formation of randomly oriented nanofibers (Figure 2.4) was observed in pure SF (100 SF) as well as in all of its combinations with SPI after electrospinning. In addition, intriguingly, some bead structures were found to be formed with 75/25 SPI/SF formulation post electrospinning. EtOH vapor treatment of obtained nanofibers led to an increase in the diameter of nanofibers (Figure 2.4, Figure 2.5) (Ramji and Shah 2014). It is likely that the water present in the EtOH aqueous solution (70% v/v) leads to expansion or swelling of the amorphous region of the protein caused due to the interruption of hydrogen bonds. This is followed by the penetration of EtOH in the expanded region and transformation of the random coil to β sheet structure. Consequently, the nanofibers swell resulting in an increase in the fiber diameter (Hu et al. 2012). Zhang et al. have reported a similar observation, wherein authors have performed SEM analysis of the aqueous EtOH solution treated SF nanofibers and found that the treatment led to a significant increase in average fiber diameter (F. Zhang, Wang, and Zuo 2010). Moreover, a similar finding has been reported by Huang et al., for water-vapor-annealed silk nanofibers (Huang et al. 2014). The respective fiber diameter calculated from SEM images is summarized in Table 2.3. In ethanol vapor non-treated electrospun mats, the diameter of fibers ranges between 30 nm to 360 nm with a minimum mean diameter of 71 ± 22 nm

for the 75/25 SPI/SF blend and maximum mean diameter of 160 ± 56 nm corresponding to the 25/75 SPI/SF blend. Whereas, in EtOH vapor treated electrospun scaffolds, the diameter of fibers range between 60 nm to 780 nm with a minimum mean diameter of 158 ± 63 nm for 100 SF and maximum mean diameter of 238 ± 107 nm of the 50/50 SPI/SF blend (Table 2.3). Moreover, the obtained electrospun nanofibrous scaffolds were found to be interconnected as well as randomly oriented, forming a porous three-dimensional network.

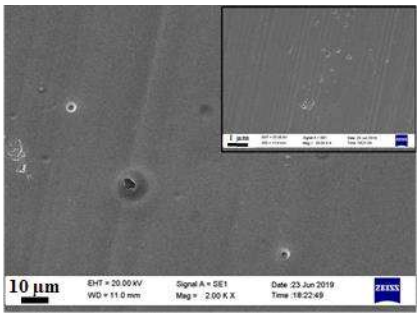

Figure 2.3 Morphological analysis through SEM photomicrograph of electrospun sheet of 100 SPI solution at different magnifications.

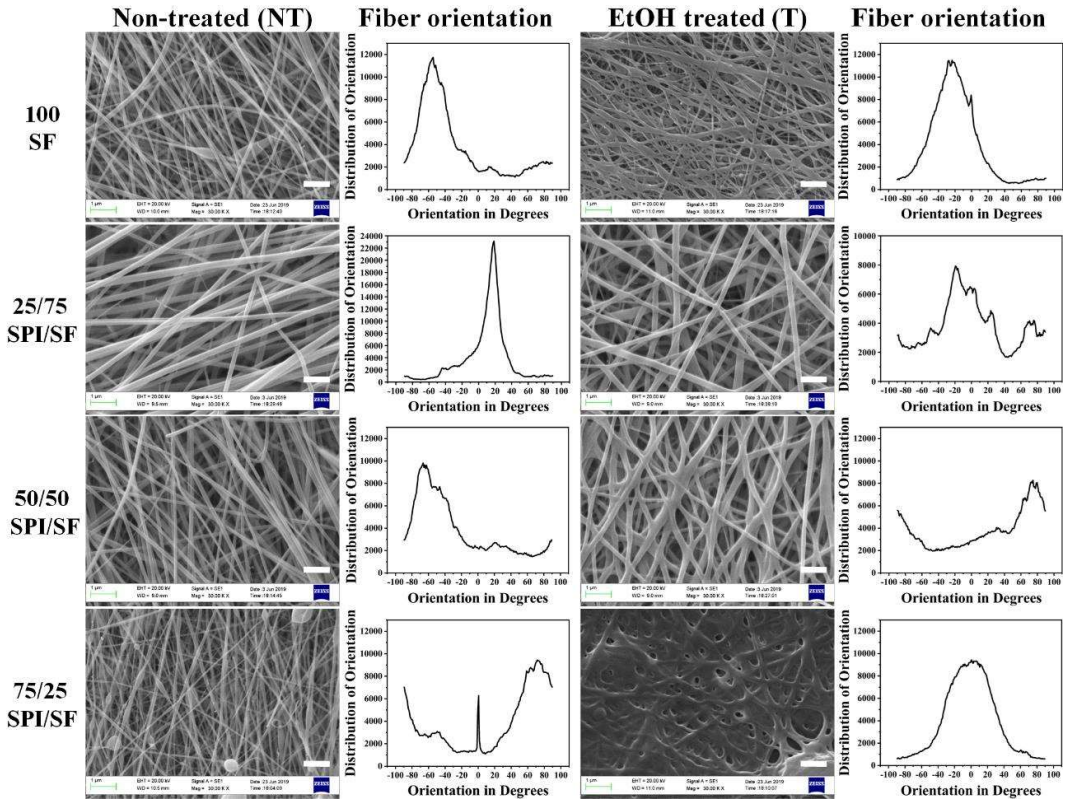

Figure 2.4 Morphological analysis through SEM photomicrographs of the prepared nanofibrous scaffolds with different SPI/SF blend compositions, namely: 100 SF, 75/25 SPI/SF, 50/50 SPI/SF, and 25/75 SPI/SF along with their respective fiber orientation graphs. Scale bar: 1 μm.

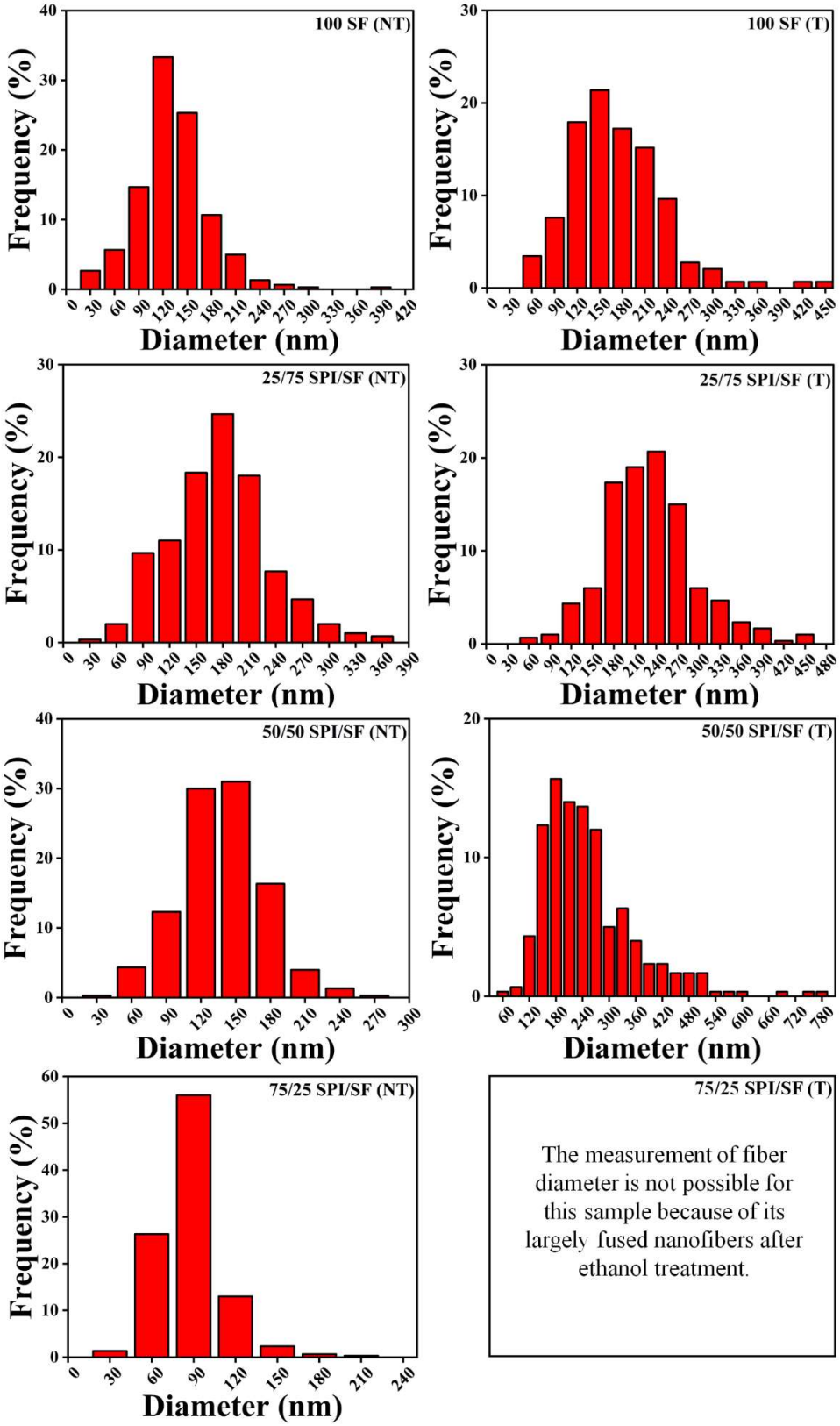

Figure 2.5 Diameter distribution of nanofibers for different compositions of nanofibrous electrospun scaffolds: 100 SF (NT), 100 SF (T), 25/75 SPI/SF (NT), 25/75 SPI/SF (T), 50/50 SPI/SF (NT), 50/50 SPI/SF (T), 75/25 SPI/SF (NT) and75/25 SPI/SF (T).

Table 2.3 Morphology, mean diameter and porosity of electrospun nanofibrous mats with various compositions.

Sample (10% w/v)	Fiber morphology	Mean diameter (nm)	Porosity (%)
100 SPI (NT)	No nanofibers formation	-	-
100 SPI (T)	No nanofibers formation	-	-
75/25 SPI/SF (NT)	Thin nanofibers with few random beads	71 ± 22	50.1 ± 0.6
75/25 SPI/SF (T)	Largely fused nanofibers after treatment	-	15.0 ± 1.2
50/50 SPI/SF (NT)	Smooth nanofibers	122 ± 36	48.7 ± 0.9
50/50 SPI/SF (T)	Thick nanofibers with fused fibers after treatment	238 ± 107	34.5 ± 6.4
25/75 SPI/SF (NT)	Smooth nanofibers	160 ± 56	51.1 ± 0.4
25/75 SPI/SF (T)	Smooth nanofibers with fused fibers after treatment	216 ± 64	43.0 ± 0.1
100 SF (NT)	Smooth nanofibers	118 ± 45	49.3 ± 0.6
100 SF (T)	Thick nanofibers after treatment	158 ± 63	40.0 ± 0.1

Adequate porosity is an essential pre-requisite for scaffold based tissue constructs. Porosity facilitates nutrient transportation, oxygen, and water diffusion to cells and helps in cell migration and growth (Varshney et al. 2019; Bonfield 2006). The porosity of all the fabricated nanofibrous ethanol non-treated electrospun mats was found to be around 50%. However, a significant drastic reduction in porosity percentage was observed in ethanol treated nanofiber mats primarily because of the increased fiber diameter during the treatment (Figure 2.6 and Table 2.3).

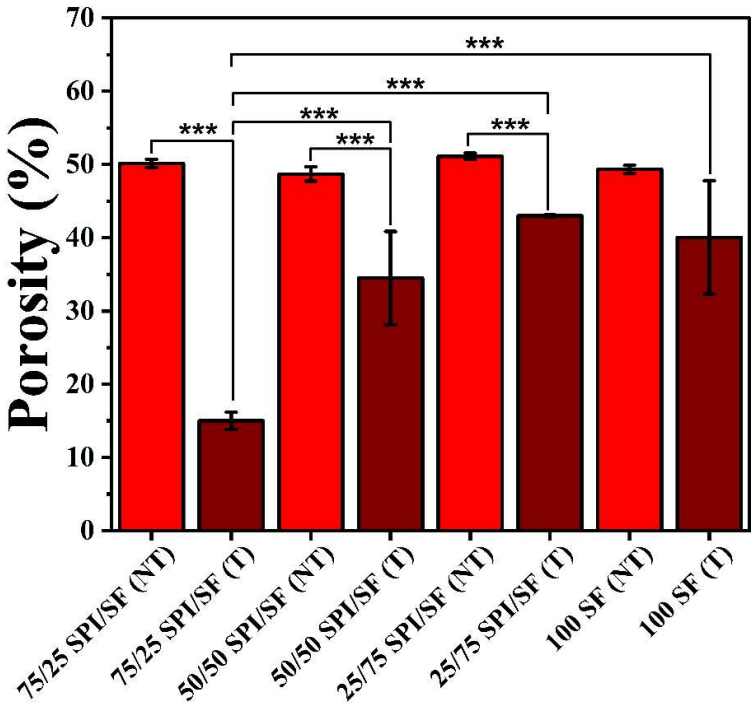

Figure 2.6 Graph depicting the porosity percentage of nanofibrous scaffolds analyzed by applying the threshold function on SEM micrographs. Values are expressed as mean ± SD (n = 5) and the level of significance as ***$p < 0.05$.

2.3.2 ATR-FTIR spectroscopic analysis of electrospun mats

The presence of respective functional groups within the electrospun nanofibers and the effect of EtOH treatment on them were analyzed by infrared analysis. The FTIR spectrum of SPI powder, 100 SPI, 100 SF, 75/25 SPI/SF, 50/50 SPI/SF, 25/75 SPI/SF (EtOH vapor treated (T) and non-treated (NT)) are shown in Figure 2.7. The major peaks of SPI powder were observed at 3279, 1630, and 1524 cm^{-1}. The first peak corresponds to the presence of amide A structure which represents NH stretching vibration. The second peak corresponds to amide I, which is a characteristic of C=O stretching vibration whereas the third peak represents amide II from N-H bending. However, for ethanol non-treated 100 SF, the main characteristic peaks for amide A, amide I and amide II were observed at 3294, 1647 and 1528 cm^{-1} respectively, where the peaks corresponding to amides I and II attribute to random coil conformation. As the SPI content increased, the peaks were

observed to be more close to 100 SPI peaks and vice versa for SF content. After 12 h of EtOH vapor treatment, major shifting was observed in the amide I and amide II peaks mainly for samples with a high SF content. In samples 100 SF(T), 25/75 SPI/SF (T) and 50/50 SPI/SF (T) these two peaks shifted to lower wavenumber, for amide I: 1647→1625, 1647→ 1625, and 1652→ 1625; amide II: 1528 → 1517, 1534 →1515 and 1540 → 1517 cm^{-1}, respectively. The EtOH treated SF containing nanofibers showed major peaks at 1625 and 1515 cm^{-1} which are specific to strong β-sheet conformation (Kim et al. 2003).

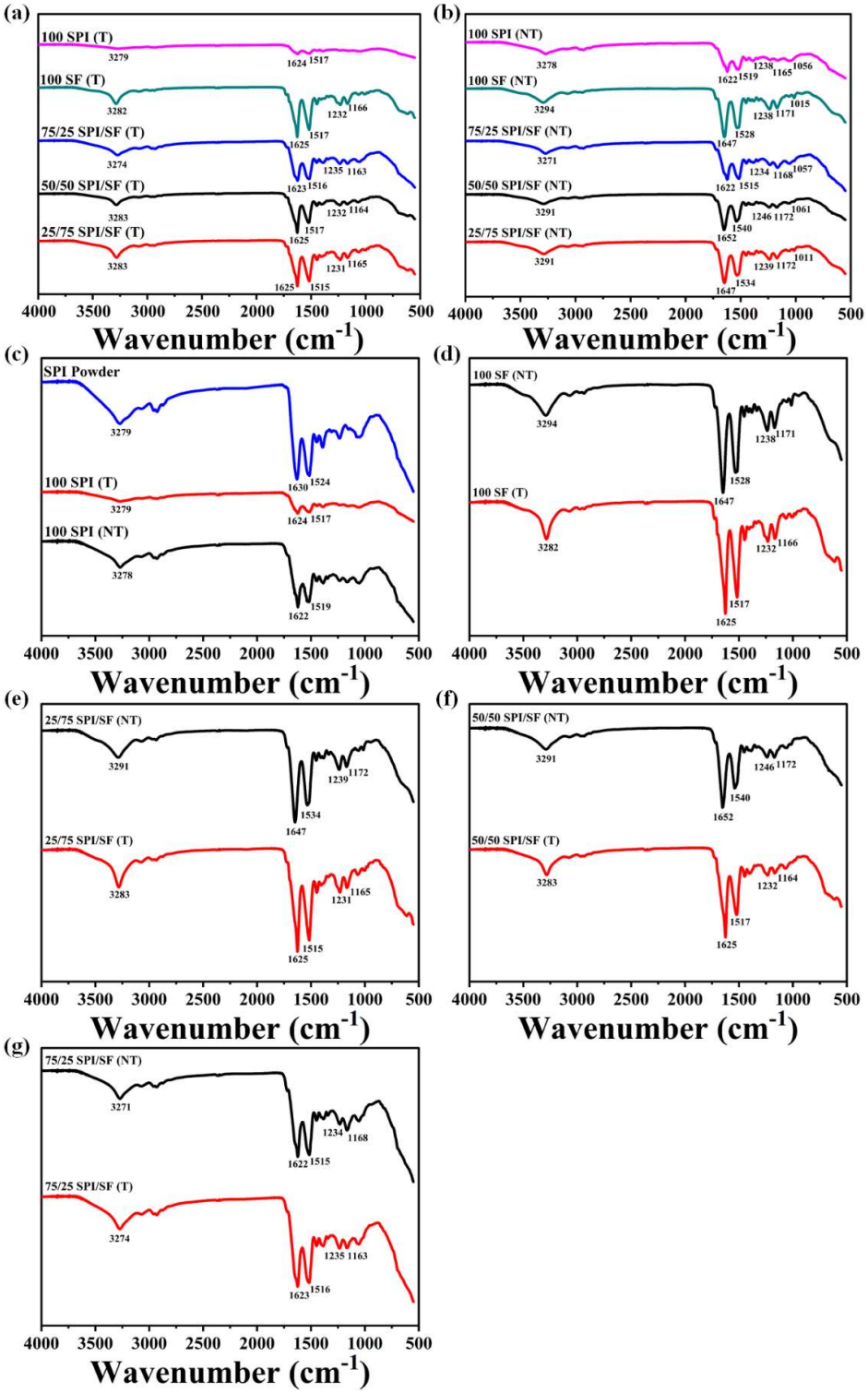

Figure 2.7 ATR-IR spectra of **(a)** SPI/SF (NT) **(b)** EtOH vapor treated SPI/SF (T) blend electrospun nanofibers. **(c–g)** Comparison between ATR-IR spectra of EtOH vapor treated and non-treated various SPI/SF blend electrospun nanofibers: 100 SPI, 100 SF, 25/75 SPI/SF, 50/50 SPI/SF and 75/25 SPI/SF.

2.3.3 Raman spectroscopy analysis

The ethanol vapor treatment leads to transformation of secondary structure from random coils to β-sheet conformation. The Raman spectra of fabricated SPI/SF blend nanofibers are shown in Figure 2.8. The major bands of 100 SF (NT) nanofibers spectra were observed at 1107 cm^{-1}, 1245 cm^{-1}, 938 cm^{-1} and 1671 cm^{-1}. In the literature (Huang et al. 2014; Marie-Eve Rousseau et al. 2004), the band about 1107 cm^{-1} has been assigned to α-helix structure (silk I) whereas the bands around 1245 cm^{-1}, 938 cm^{-1} have been assigned to random coil structure and around 1671 cm^{-1} for β-turns. However, in Figure 2.8 (a), the major bands of 100 SF (T) nanofibers were observed at 1088 cm^{-1}, 1227 cm^{-1} and 1665 cm^{-1}, which confirms the β-sheet conformation in nanofibers. Moreover, similar spectra were observed for 25/75 SPI/SF and 50/50 SPI/SF ethanol vapor treated (T) nanofibers as obtained for 100 SF (T) nanofibers. The results suggest that the ethanol treatment induces the crystallinity of nanofibers by transforming the secondary structure from random coils to β-sheets.

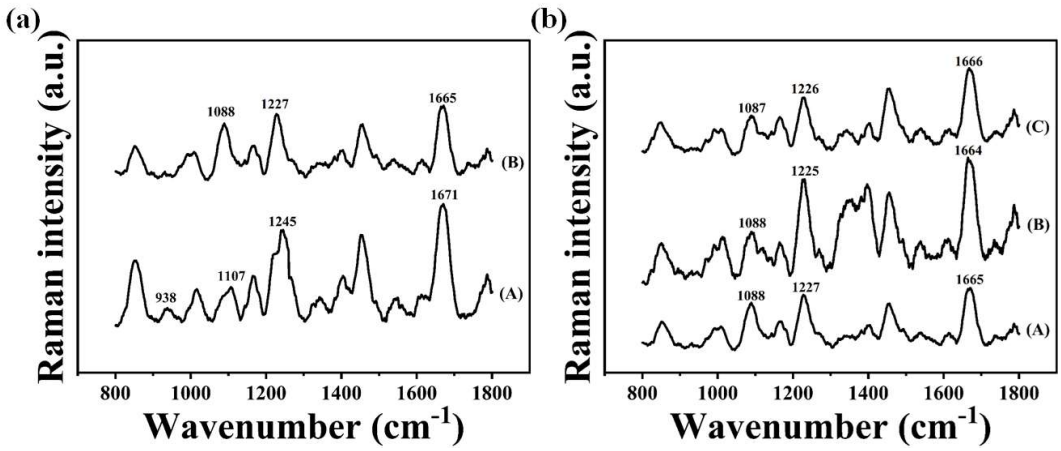

Figure 2.8 Raman spectra of electrospun SPI/SF nanofibers: **(a)** ethanol vapor treated (T) and non-treated (NT) nanofibers (A) 100 SF (NT) (B) 100 SF (T) and **(b)** ethanol treated (T) all the fabricated nanofibers (A) 100 SF (B) 25/75 SPI/SF (C) 50/50 SPI/SF.

2.3.4 Swelling capacity

The swelling capacity of the prepared nanofibrous scaffolds was examined in terms of percentage weight gain after being immersed in PBS over a period of 48 h. The scaffolds showed an improvement in the stability as well as increment in the water retention capacity after EtOH vapor treatment due to the structural transition from random coil to β sheet. Treated scaffolds gained more weight in comparison to their non-treated forms (Figure 2.9). It has been reported that ethanol or methanol vapour treatment leads to dehydration as well as an increase in the beta sheet structure of the silk protein; resulting in a significantly greater imbibe of water during hydration (Lawrence et al. 2010). Hence, a higher level of weight gain percentage is observed in the treated nanofibers in comparison to their non-treated counterparts. Moreover, this change in retention capacity was further improved with an increase in the SPI content of nanofibers. The non-treated 50/50 SPI/SF, 75/25 SPI/SF and 100 SF scaffolds achieved weight gains of 735 ± 51.2%, 655 ± 99.1% and 485.4 ± 67.6%, respectively, from their initial weights after being immersed in PBS solution for 48 h. While the treated scaffolds 50/50 SPI/SF, 75/25 SPI/SF and 100 SF achieved 1054.5 ± 92.6%, 855.1 ± 7.2% and 815 ± 21.2% weight gains, respectively, in which 50/50 SPI/SF scaffold showed the highest percentage of weight gain among them.

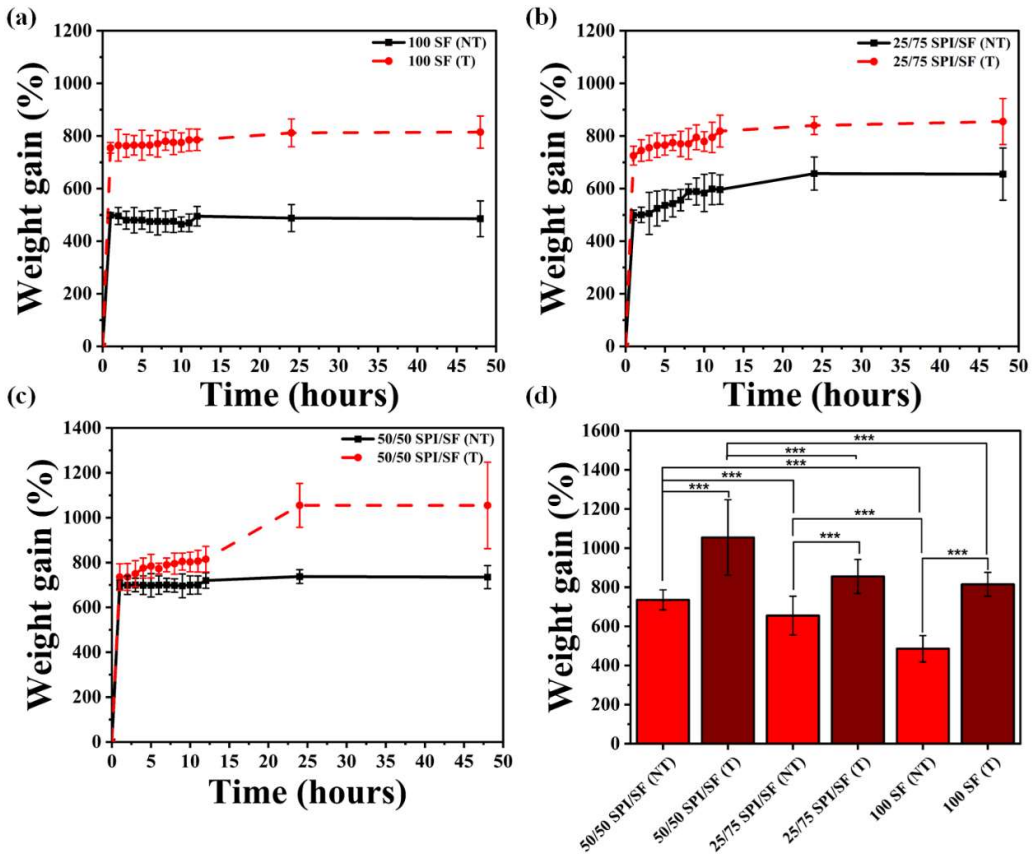

Figure 2.9 Graph shows weight gain percentage of different nanofibrous scaffolds of various ratios of SF and SPI, before and after ethanol vapor treatment in PBS at a room temperature (25 °C) (a) 100 SF (b) 25/75 SPI/SF (c) 50/50 SPI/SF electrospun scaffold (d) comparison of weight gain percentage of nanofibrous scaffolds. Values are expressed as mean ± SD (n = 3) and the level of significance as ***$p < 0.05$.

2.3.5 Stability and degradation of electrospun nanofibers

The stability and degradation of a biomaterial is another property that decides its suitability for TE applications. The evaluation of the stability of the fabricated electrospun nanofibrous sheets was performed at the physiological as well as at room temperature. The nanofibrous sheets were cut into discs of 10 mm diameter and soaked in PBS (pH 7.4) for 13 days at room temperature. The electrospun scaffolds were found to be quite stable and no significant degradation was evident when observed using digital imaging, up to 13 days of continuous soaking in PBS (Figure 2.10(a)). Samples were found firm

enough to be held using forceps even after 10 days of continuous soaking in an aqueous medium (Figure 2.10(b)). To simulate the behavior of nanofibers in vivo, in vitro degradation study in a lysozyme-containing solution was conducted because of the presence of this enzyme in various body fluids including tears and serum (Ren et al. 2005). Although in physical appearance there was no clear deterioration observed through digital imaging (Figure 2.10(c)), SEM analysis revealed that all the samples except 100 SF EtOH treated scaffolds lost their fiber morphology after 20 days of incubation in a lysozyme-containing solution at 37˚C, (Figure 2.10(d)). In non-treated samples, it was observed that the porous fiber network collapsed and fused together during degradation. In treated samples, fiber structures were found to be swollen and deteriorated to some extent; however, the 100 SF samples demonstrated a negligible amount of structural deterioration and degradation. Furthermore, it was observed that the addition of SPI enhanced the rate of degradation of the SF nanofibers which is an essential property for skin TE applications. Moreover, we found that rate of degradation of the nanofibers is directly proportional to the content of SPI in the fabricated samples. In particular, 100 SF, 25/75 SPI/SF and 50/50 SPI/SF showed percentage weight losses of 12.5 ± 1.4%, 14.8 ± 1.2% and 34 ± 2.8%, respectively, from their initial weights. The same trend was observed in non-treated samples.

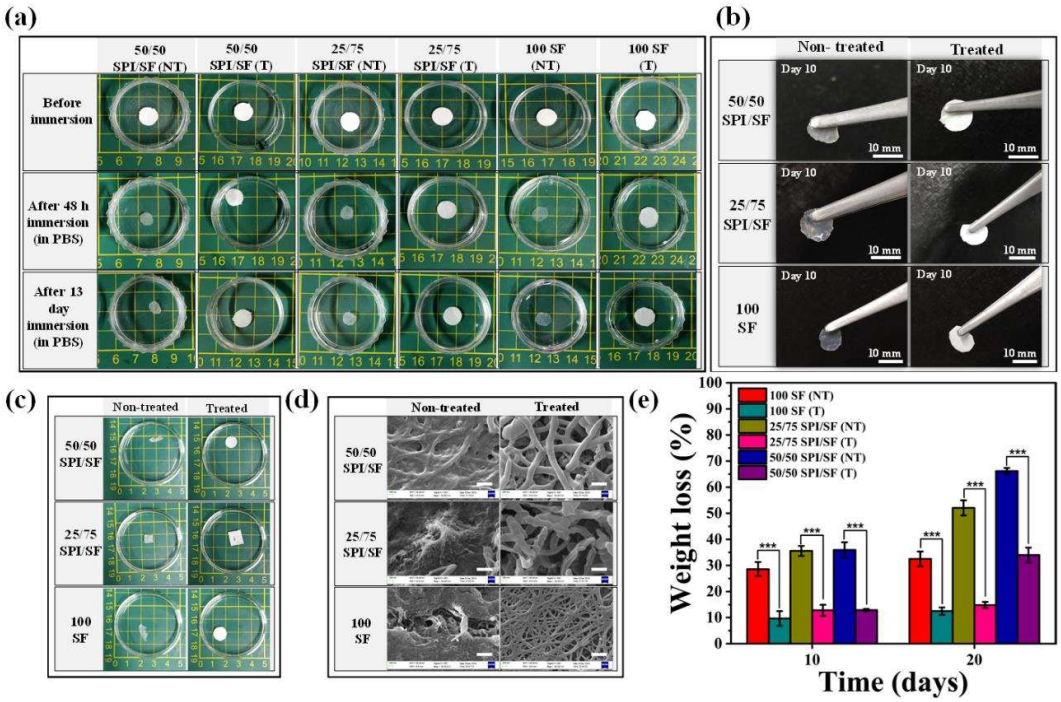

Figure 2.10 Represents (a) digital images depicting stability of prepared nanofibrous scaffolds in PBS at a room temperature (b) digital images of scaffolds held through forceps after 10 day immersion in PBS at 37 °C, (c) and (d) digital and SEM micrographs of electrospun samples, respectively, after 20 days degradation in lysozyme containing solution at 37 °C (e) graph shows weight loss percentage of samples over 20 days of immersion in lysozyme-containing solution at 37 °C. Values are expressed as mean ± SD (n = 3) and the level of significance as ***$p < 0.05$. Scale bar is 800 nm for SEM images.

2.3.6 Transparency percentage of the fabricated nanofibrous scaffolds

The non-treated (NT) nanofibrous discs were observed to be transparent, and their diameters were found to be reduced when placed in the aqueous solution, depicting a significant shrinkage of the scaffold. On the other hand, EtOH vapor treated (T) nanofibrous discs remained opaque and no variation in size was observed when immersed in PBS (Figure 2.11(a)). In visible light, the transparency of the non-treated nanofibers was found to be significantly higher in comparison to that of the ethanol treated samples (Figure 2.11(b)). This is because of the increased crystallinity of the fibers after ethanol treatment as evident from the above FTIR results. The graph represents a 72 ± 7.9% transparency for 100SF (NT) which is more than 44 ± 9.6% for 25/75 SPI/SF (NT) and

38 ± 10.9% for 50/50 SPI/SF (NT) samples. The non-treated sheets exhibited transparency in between 40% to 70%, which is quite suitable for various TE applications such as corneal tissue construct, skin tissue construct, etc.

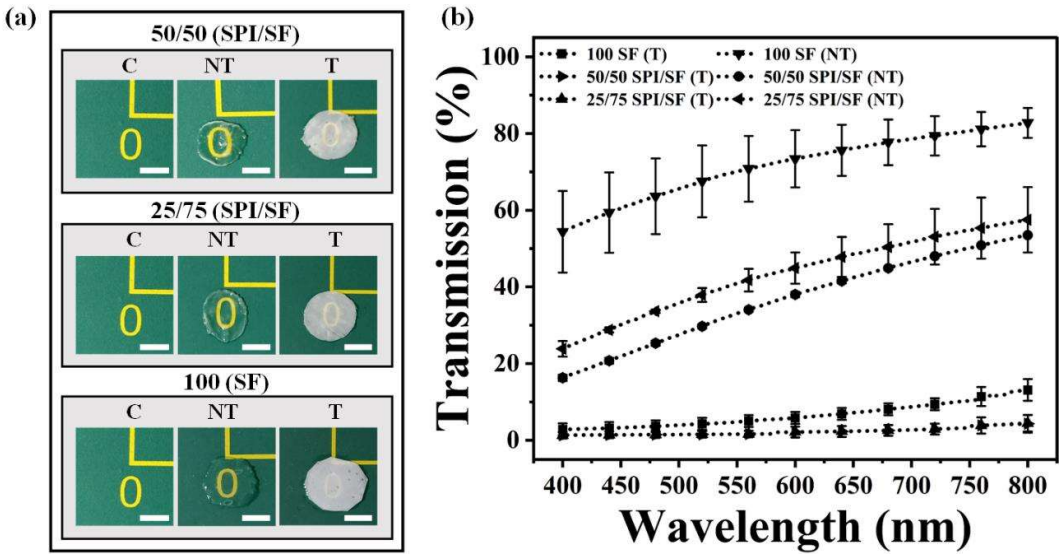

Figure 2.11 Transparency of different nanofibrous scaffolds of various ratios of SF and SPI before (NT) and after ethanol vapor treatment (T) in PBS at a room temperature (25 °C) (a) digital images of samples showing visual transparency (b) graph shows percentage of light transmission through the samples. Scale bar: 4 mm. Values are expressed as mean ± SD (n = 3).

2.3.7 Thermal stability of the fabricated nanofibrous sheets

Thermogravimetric analysis of the ethanol treated as well as untreated electrospun nanofibers was performed, and the temperature, from where a sharp loss in weight took place called the degradation temperature was measured for each sample. The degradation temperature of non-treated 100 SF, 25/75 SPI/SF, and 50/50 SPI/SF were recorded to be 218˚C, 238˚C and 229˚C, respectively, which after ethanol vapor treatment shifted to 244˚C, 250˚C and 247˚C, respectively (Figure 2.12). This shifting in degradation temperature depicts that β sheet transformation induced by ethanol treatment leads to an increase in crystallinity of the nanofibers and in turn the stability of the nanofibers.

However, no considerable difference was observed between the 100 SF, 25/75 SPI/SF, and 50/50 SPI/SF samples. Moreover, similar amount of residues was observed in all the samples i.e. 40-43% at 500˚C.

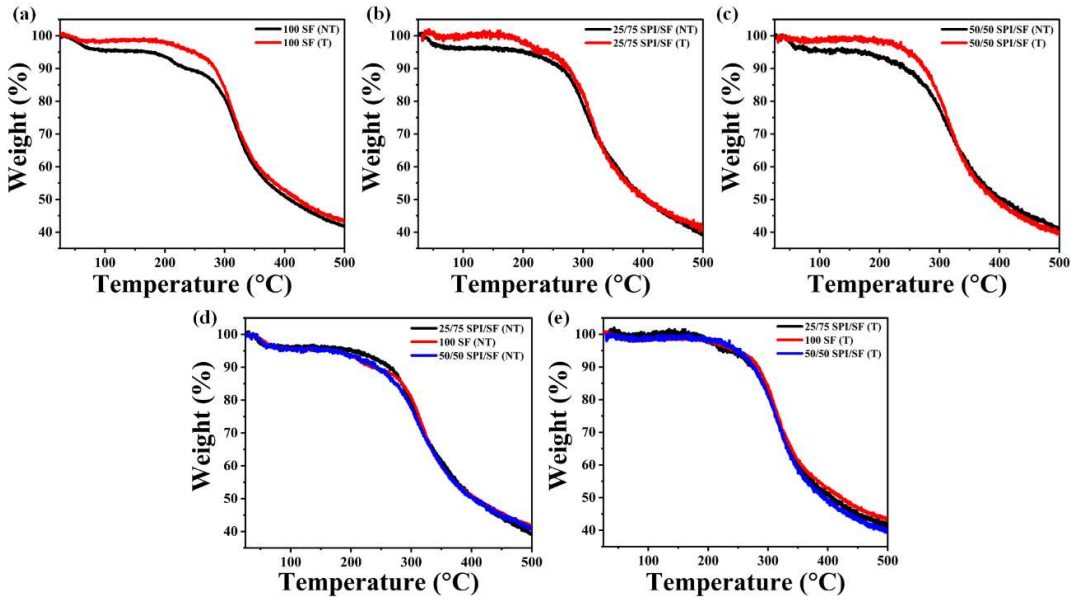

Figure 2.12 TGA curve of EtOH vapor treated (T) and non-treated (NT) various SPI/SF blend electrospun nanofibers: (a) 100 SF (b) 25/75 SPI/SF (c) 50/50 SPI/SF, (d) non-treated samples (e) treated samples.

2.3.8 Cytocompatibility of the fabricated nanofibrous scaffolds

Cell attachment and spreading are the crucial factors of any tissue engineered skin substitute for tissue regeneration. The suitability of the prepared nanofibrous scaffold for in vitro cell culture was microscopically analysed by culturing the L929-RFP (fibroblast) and B16F10 (melanocytes) cells on the fabricated sheet for 7 days (Figures 2.13 and 2.14). Fluorescent microscopy demonstrated that both cell types were growing remarkably well and reached confluency by the 7^{th} day of culture. The level of cell confluency in a particular scaffold was found to be variable depending upon the type of cells being cultured. The L929-RFP cells were found to be more confluent in 25/75 SPI/SF and 50/50

SPI/SF samples (both T and NT) in comparison to 100 SF (Figure 2.13). While, the B16F10 cells were observed to be more confluent in 100 SF and 25/75 SPI/SF samples than the 50/50 SPI/SF samples (Figure 2.14).

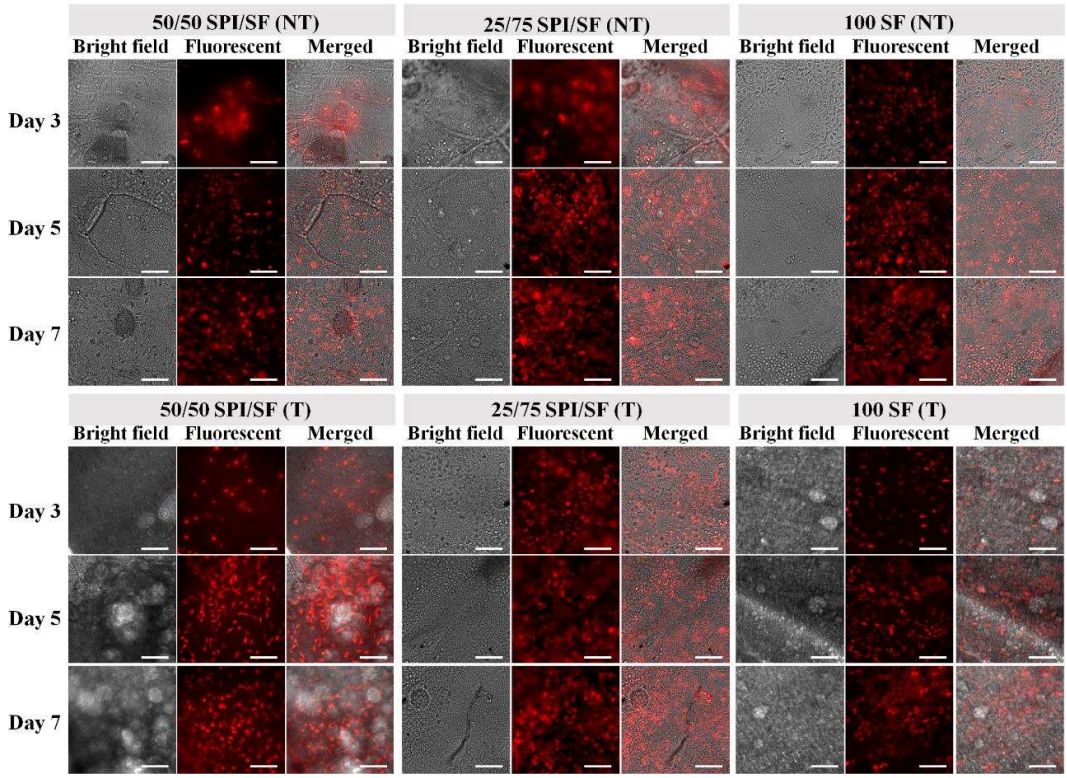

Figure 2.13 The above panel of images represents the culture of L929-RFP (fibroblast) Left: 50/50 SPI/SF, middle: 25/75 SPI/SF and right: 100 SF for over a period of 7 days. Scale bar is 100 μm for brightfield, fluorescent and merged images.

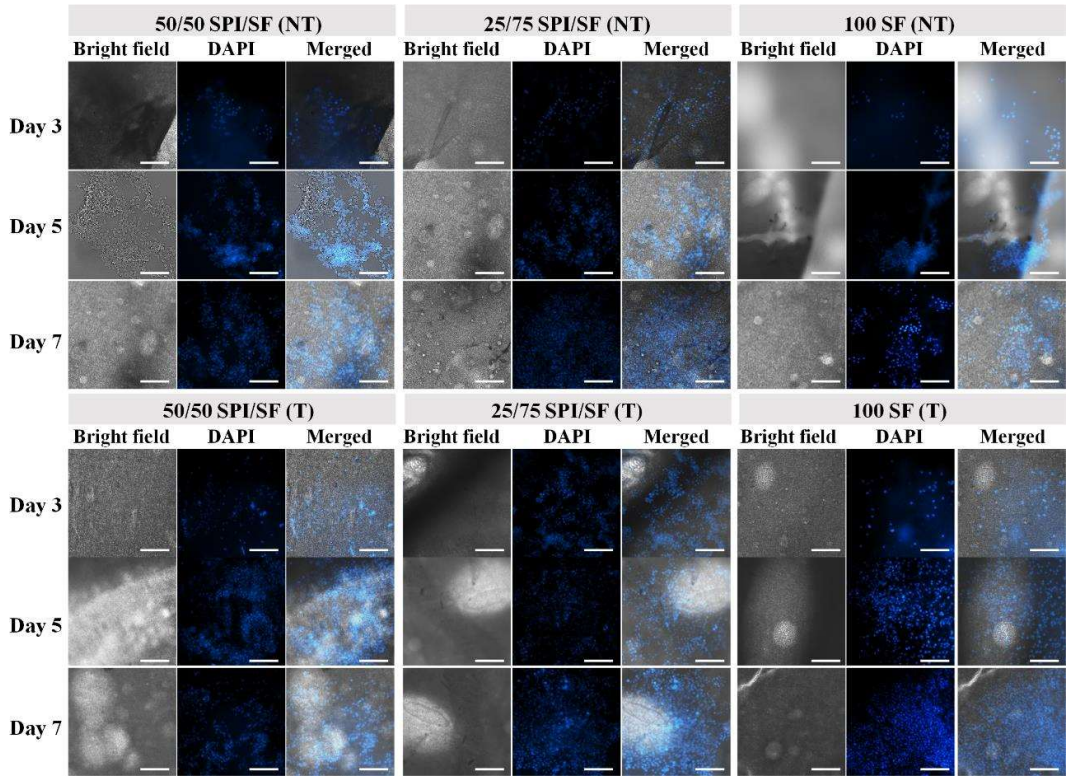

Figure 2.14 The above panel of images represents the culture of B16-F10 (melanocytes) cells within the nanofibrous scaffolds. Left: 50/50 SPI/SF, middle: 25/75 SPI/SF and right: 100 SF for over a period of 7 days. Scale bar is 100 μm for brightfield, fluorescent and merged images.

When estimated using MTT assay, an increase in the cellular viability of both types of cells (NIH-3T3 fibroblast and B16F10 melanocyte cells) was observed in all the samples up to 4 days of culture (Figure 2.15). A significant difference was observed in the viability percentages of NIH-3T3 fibroblast cells that were 44.1 ± 9.4%, 76.8 ± 9.8% and 82.1 ± 12.1%, when cultured on 100 SF (NT), 25/75 SPI/SF (NT), and 50/50 SPI/SF (NT), respectively. With a cellular growth greater than 70% by the 4th day of cell culture within the nanofibrous scaffolds, both 25/75 SPI/SF (NT), and 50/50 SPI/SF (NT) ethanol non-treated scaffolds were found to be suitable for the viability of fibroblast cells. Ethanol treated samples showed relatively higher cellular viability than the ethanol non-treated samples with individual percentages of 79.8 ± 4.5%, 79.3 ± 16.1% and 81.2 ± 5.6% for

100 SF (T), 25/75 SPI/SF (T) and 50/50 SPI/SF (T), respectively. However, no significant difference in the viability percentage was observed among them. Together, these observations suggest that the rate of cell proliferation increases with the increase of SPI content in the blends; inferring that soy protein plays an important role in enhancing the cellular viability of blends. In contrast to NIH-3T3 fibroblast cells, B16-F10 cells behaved quite differently though (Figure 2.15 (c)). In the case of B16-F10 cells, the percentage of cellular viability significantly decreased with the increase in SPI content in the scaffolds (Figure 15(b)) with individual values 39.52 ± 3.8, 25.9 ± 3.9 and 15.11 ± 2.6 for 100 SF (NT), 25/75 SPI/SF (NT) and 50/50 SPI/SF (NT), respectively. A similar trend was observed for ethanol treated samples i.e. 100 SF (T), 25/75 SPI/SF (T) and 50/50 SPI/SF (T) with values 44.66 ± 8.4, 46.05 ± 5.18 and 27.35 ± 4.5, respectively. This is most likely due to the presence of anticancer peptides in SPI as also reported in the previous study (Shidal et al. 2017).

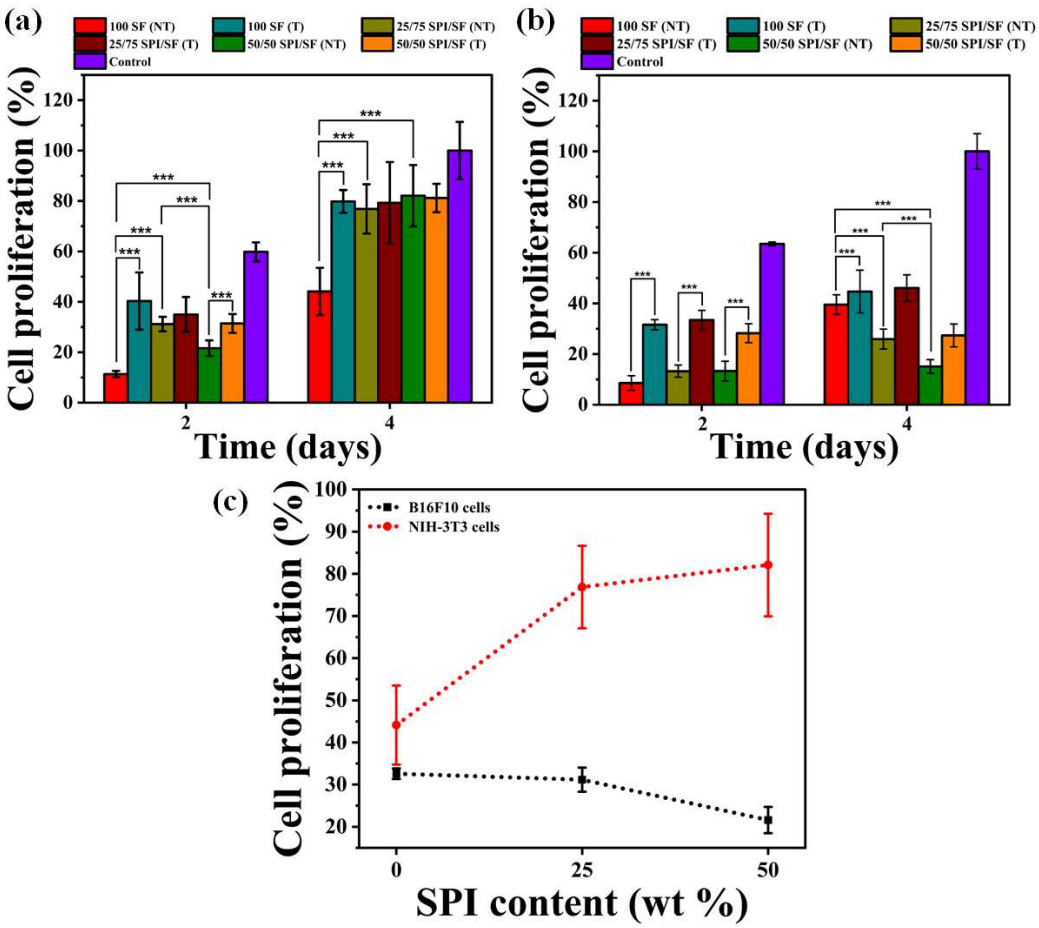

Figure 2.15 The figure illustrates the percentage cellular viability of (a) NIH-3T3 cells and (b) B16-F10 cells for 2 and 4 days and the compatibility of the nanofibrous scaffolds determined by MTT assay (c) comparative cellular viability percentage of NIH-3T3 cells and B16-F10 cells within nanofibrous scaffolds with respect to ratio of soy protein isolate (SPI). In MTT assay experiment, absorbance for the 4th day culture of positive control was taken as reference OD for all the samples. Values are expressed as mean ± SD (n = 3) and the level of significance as ***$p < 0.05$.

The cell adhesion and morphology of 48 h cultured NIH-3T3 cells on samples were also studied using SEM images (Figure 2.16). From these images, it was observed that all the samples promoted cell attachment and proliferation while no visual (qualitative) difference was observed in cell spreading area and morphology. Thus, these results indicate that the prepared nanofibrous scaffolds are cytocompatible and favorable for cell adhesion and facilitate uniform cellular growth within the 3D network.

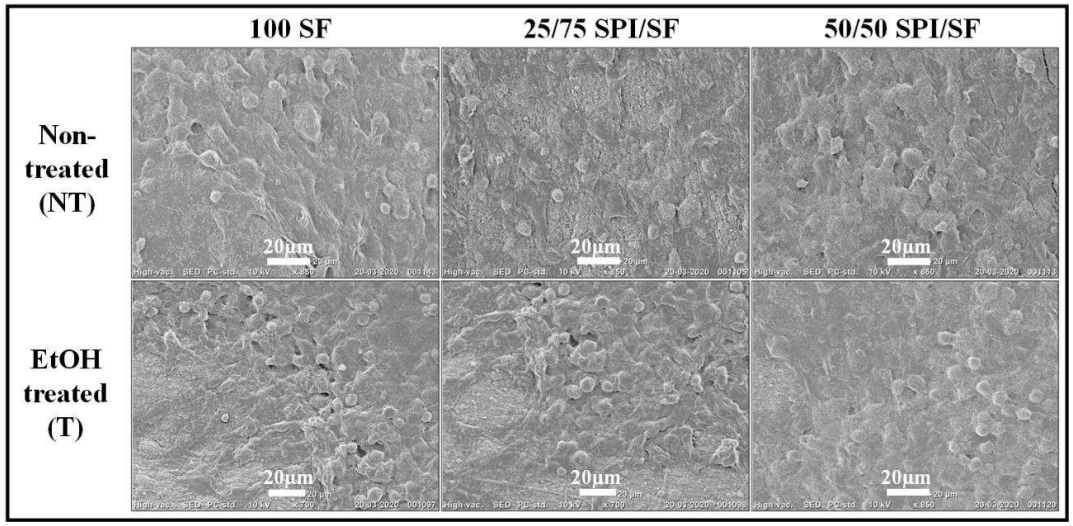

Figure 2.16 The figure illustrates SEM images of NIH-3T3 (fibroblast) cells cultured on fabricated nanofibrous scaffolds. Scale bar is 20 µm for SEM images.

2.3.9 In vivo wound healing

The aforementioned characterization of prepared electrospun nanofibrous scaffold suggested its applicability for skin TE and prompted us to check its suitability for in vivo wound healing. We therefore studied the healing of the surgically induced wound in rat over a period of 14 days in the presence (treated) as well as in absence (untreated) of the fabricated scaffold. In the case of a 50/50 SPI/SF (T) treated group, it was observed that scaffold excellently adhered to the wound surface and utterly degraded over a period of time. The sample treated rat group showed faster healing in comparison to the rat group without any treatment (sham) (Figure 2.17). The reason behind the faster healing might be the native ECM-like structure provided by the nanofibrous scaffold i.e., adhesion moieties present on the proteins and peptides arising due to the degradation of soy protein (Thirugnanaselvam, Gobi, and Arun Karthick 2013; Bhardwaj and Kundu 2010a). On day 11, 50/50 SPI/SF (T) treated group obtained almost 100% wound closure, whereas the untreated group obtained up to 80% only. During the overall 14 days period of the

experiment post-operation, no single animal showed any adverse effects such as fluid confinement, granulation tissue bleeding, sepsis, infection, etc. All the animals were alive throughout the experiment and sacrificed after day 14. The histological difference in granulation tissue of sample treated groups and untreated groups was examined through H & E staining after day 14 (Figure 2.16(c)). 50/50 SPI/SF (T) nanofibrous scaffold treated group showed full re-epithelialization. The epidermis was infiltered by keratinocyte cells and a thick layer structure was made with collagen deposition in the dermal layer, which depicted complete wound healing. The untreated group showed less re-epithelialization with moderate collagen deposition in the dermal layer.

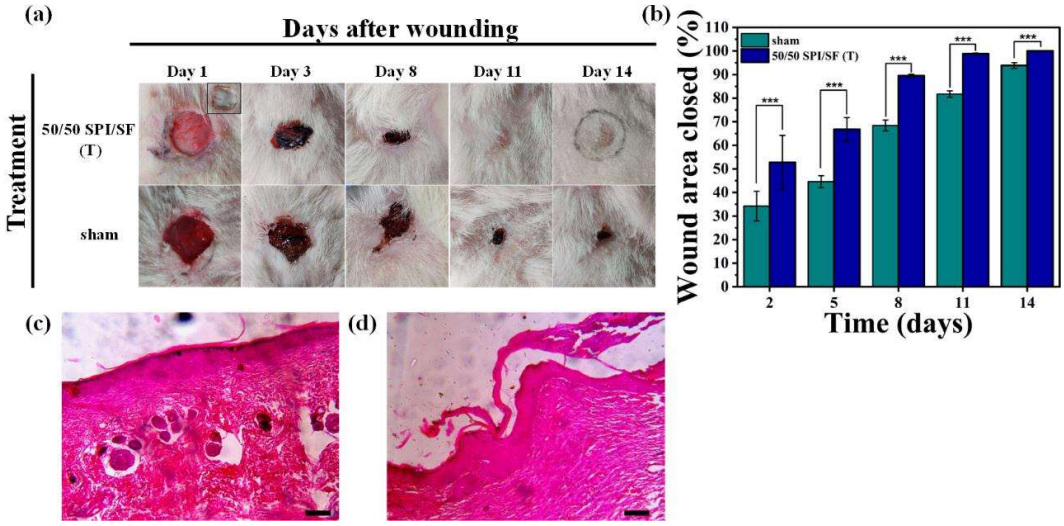

Figure 2.17 Shows in vivo wound healing (a) digital photographs of full thickness wound closure on day 1, 3, 8, 11 and 14 (b) graph depicts a comparison of wound area closed percentage of treated and sham (untreated) groups (c) and (d) H&E staining image of the histological section of 50/50 SPI/SF (T) and sham, respectively, after 14 days. Values are expressed as mean ± SD (n = 3) and the level of significance as ***$p < 0.05$. Scale bar: 100 μm.

2.4 Discussion

The objective of this work was to fabricate and examine the nanofibrous SPI/SF protein blend scaffolds as a wound dressing material. Researchers have investigated that some

specific amino acids are required for proper wound healing and tissue regeneration processes such as glutamine and arginine. Glutamine is used as an energy source by inflammatory cells for their proliferation during the wound healing process, whereas arginine is crucial for efficient immune function and wound restoration (MacKay and Miller 2003; Yoshie-Stark, Wada, and Wäsche 2008). SPI contains a high amount of these two amino acids and cell adhesion moieties (Jeong et al. 2007). Our study explored the SPI blends with SF as a co-blending polymer since both SPI and SF are promising polymers in the TE field (R. Silva et al. 2014; Tansaz et al. 2018; Schneider et al. 2009). We have elucidated the process of development of an SPI/SF blend based electrospun nanofibrous scaffold with different ratios in formic acid. There are quite a few studies reported in the literature related to the exploration of soy protein synergy with diverse natural polymers for the production of nanofibrous scaffolds; some of these include a blend of soy flour-gluten (Lubasova, Mullerova, and Netravali 2015), zein-SPI (Phiriyawirut et al. 2008), and SPI-lignin (Salas et al. 2014). Therefore, we found it addressable to explore the soy protein with other natural polymers to improve or modulate the limitations of natural polymer for TE applications such as to develop a tunable biodegradable natural polymeric scaffold that can mimic the ECM architecture. Silk was added to expedite fiber formation and improve the mechanical strength of the scaffold.

Results revealed that except 100 SPI, all the blend solutions (75/25 SPI/SF, 50/50 SPI/SF, 25/75 SPI/SF, and 100 SF) were successfully electrospun into the nanofibrous scaffold. SEM analysis showed that pure SPI in formic acid was not electrospinnable as also observed by Phiriyawirut et al. that SPI alone was not able to produce fibers in either acetic acid or formic acid (Phiriyawirut et al. 2008). Ramji K. et al. reported the production of electrospun nanofibers for TE applications only when pure SPI was used in combination with a copolymer PEO (Ramji and Shah 2014). The formed nanofibrous

mats were found to be little brittle, and their brittleness increased with an increase in the SPI ratio in the prepared formulation.

The pure SPI powder as well as electrospun 100 SPI with or without EtOH vapor treatment upon ATR-FTIR spectroscopic analysis gave amide I and amide II specific peaks in the same range (between 1622 - 1630 cm^{-1} and 1517 - 1524 cm^{-1}) (Figure 2.7) which indicates that the electrospinning and EtOH treatment do not affect the native structure of SPI protein. From Figures 2.7 and Figure 2.8, we observed that the secondary structure of SF in prepared nanofibers was converted to β sheet structure (silk II) from random coil structure (silk I) because of 12 h EtOH vapor treatment (Fan et al. 2012). These results are in agreement with the previous studies reported by Fan et al. (Fan et al. 2012), Ning et al. (Ning et al. 2018), Chen et. al. (J.-P. Chen, Chen, and Lai 2012) and Zhang et al.(F. Zhang, Wang, and Zuo 2010) on the fabrication of SF nanofibers for TE applications. In particular, these groups have conducted various analyses using the techniques such as ^{13}C-NMAR, FTIR, X-ray diffractometry, thermogravimetry (TG), differential thermogravimetry (DTG) and DSC analyses to demonstrate that EtOH vapour treatment induces crystallinity of SF nanofibers by transforming the secondary structure from random coils to beta sheets.

From the FTIR and Raman spectral analysis, it can be inferred that EtOH treatment transforms the silk I conformation into silk II conformation and thereby leads to an increase in the crystallinity of the nanofibrous scaffolds. Furthermore, a drastic reduction in the transparency of SPI/SF electrospun mats was observed after EtOH vapor treatment; most likely due to the fact that semicrytalline or crystalline materials are known to be majorly opaque and the transparency therefore generally decreases as the crystallinity of the material increases (Ahmad et al. 2010). In particular, the transparency of any

crystalline material is dependent to a certain extent on the size of spherulites. These complex polycrystalline bodies can scatter light and lead to the reduction in the transparency of the material with size of these bodies (De Santis and Pantani 2013). The properties of a material such as permeability, hardness, mechanical, chemical, optical, thermal and stability are substantially influenced by its crystallinity. The outcomes of water retention assay depict that the increase in SPI content of SPI/SF blend significantly favors the water retention capacity of the nanofibrous scaffolds. Soy protein swells when it absorbs water, which is the most desired property of skin TE scaffolds that facilitate absorption of the excess wound exudate. This property can be attributed to the presence of a high percentage of charged amino acids majorly negatively charged like aspartic and glutamic acid and low content of hydrophobic amino acids such as leucine in soy protein (Vu Huu Thanh and Kazuo Shibasaki 1977). The high liquid retention capacity of the scaffold might create a moist microenvironment over the wound skin tissue, which will induce fast healing. Vanessa J. et al. reported that moist microenvironment accelerates the rate of epithelialization and also enhances the healing through stimulating the inflammatory phase by the moisture itself (Jones, Grey, and Harding 2006). Xu et al. developed SPI and PEO based nanofibers by utilizing 1,1,1,3,3,3-hexafluoro-2-propanol as a solvent. They showed excellent hydrophilicity with nanofibers ranging between 200 and 300 nm (Xu et al. 2012).

SPI has some limitations such as low mechanical properties and inferior hydrolytic stability. To overcome these limitations of SPI, researchers have utilized a blend of SPI with synthetic polymers (Cho, Netravali, and Joo 2012; J. Zhang et al. 2006; F. Chen and Zhang 2009). On the other hand, SF suffers from slow degradation and poor cell proliferation (Rockwood et al. 2011). Many studies were conducted to develop SF based electrospun hybrid nanofibers in pursuance of enhancing wettability, degradation, cell

adhesion and proliferation (Carrasco-Torres et al. 2019; Yoo et al. 2008). Therefore, in this study, we fabricated a blend of SPI and SF proteins to obtain a nanofibrous scaffold to overcome the above mentioned limitations of individual proteins. Accordingly, we obtain a novel protein blend with good spinnability along with other desired combined properties of constituent proteins such as high water retention capacity, excellent cellular proliferation and moderate biodegradation rate with good stability. SPI is not capable of producing strong fibers on its own which limits its widespread applications. On the other hand, silk has outstanding mechanical properties. Therefore, in this study, SF was used as a carrier polymer in order to make SPI electrospinnable and to offer the required level of strength. The mechanical properties of SF mats were further improved significantly by ethanol treatment due to the formation of β-sheets (Liu et al. 2015). This is because the physicochemical properties of SF fibers strongly depend on its molecular conformation and crystallinity. However, the increased β -sheet content corresponds to enhanced stiffness of silk based materials (Lawrence et al. 2010) and hence, as the crystallinity (β-sheet content) of SF based materials increases, they become more brittle (Huang et al. 2014). A similar observation has been reported for methanol treated pure silk (100% silk) film by DeFrates et al. (DeFrates et al. 2017). Additionally, SPI based scaffolds generally suffer from brittleness limitation and could not be successfully tested for their tensile properties. Cho and colleagues demonstrated that an electrospun fibrous mat with a high SPI amount was discovered to be brittle, and the strength of the mat could not be determined since it broke when it was clamped (Cho, Netravali, and Joo 2012). Because of these reasons, in this study, mechanical characterization of the SPI/SF scaffolds could not been performed. Nevertheless, we anticipate that the addition of SF and EtOH vapour treatment enhanced the stability and in turn the mechanical strength of the fabricated electrospun nanofibers. In the literature, an increase in the mechanical strength of

SPI/PVA electrospun nanofiber mats with an increase in the content of PVA has been reported by Cho et al (Cho, Netravali, and Joo 2012). In the future, this limitation may be overcome by utilizing some plasticizers during the fabrication process such as glycerol, since, glycerol- plasticized SP films have been shown to possess a flexible character and low tensile strength (Tian et al. 2011).

MTT and cytocompatibility studies also suggest that the addition of soy protein to SF enhances its cellular biocompatibility towards mammalian cells by providing cell adhesion moieties. A steady increase was observed in the percentage of cellular viability of fibroblast cells with an increase in the amount of SPI. On the other hand, when we cultured B16-F10 melanoma cells on nanofibrous scaffolds, we observed a noticeable decrease in the percentage of cellular viability with respect to an increase in the SPI content of the scaffold. A significant decrease in cellular proliferation can be attributed to the anticancer property of soy protein. In literature, it has been reported that soy protein has properties like antioxidative (Singh, Vij, and Hati 2014; Y.-C. Wang, Yu, and Chou 2006), anticancerous (Singh, Vij, and Hati 2014; Mejia and Lumen 2006; W. Wang et al. 2008; Lule et al. 2015; Pabona et al. 2013), immunostimulatory, anti-inflammatory and antihypertensive properties (Chatterjee, Gleddie, and Xiao 2018). SPI contains high concentration of lunasin which is a cancer preventive peptide of 43 residues with an RGD cell adhesion motif followed by nine aspartic acid residue at C-terminal (Gonzalez de Mejia et al. 2004). Many studies have reported that lunasin reduces the occurrence of skin tumors up to 70% in the SENCAR mice skin cancer model (Jeong et al. 2007; Gonzalez de Mejia et al. 2004; Galvez et al. 2001; Lam, Galvez, and de Lumen 2003). Shidal C et al. demonstrated that both in vivo and in vitro lunasin suppresses the associated metastasis activities in melanoma cancer-initiating cells (using B16F10 cells) (Shidal et al. 2017).

The prime objective of wound dressing is to achieve fast healing without any adverse effect. Our SPI/SF blend electrospun nanofibrous scaffold provides a promising alternative for a permanent wound dressing material. The efficacy of nanofibers was evaluated by examining the wound closure rate in the presence and absence of 50/50 SPI/SF (T) treated electrospun scaffold. Wound healing was found quicker in the presence of scaffold compared to in its absence. Har-el et al. developed a soy protein-based electrospun scaffold as a wound dressing and investigated its efficiency for wound healing on Yorkshire pigs. They observed a strong sign of epithelialization in SPI based scaffold treated wounds which was not present in control wounds. Besides, they also observed the presence of hair follicles and sweat glands in a treated wound and their absence in the control group after four weeks (Har-el et al. 2014). In another study, it has been reported that the moist environment provided by soy protein blend nanofibers promotes the rate of wound healing in female Wistar rats compared to the control group. The high content of glutamine in SPI was reasoned for the fast healing of wound as the cells utilize it as an energy source for growth and proliferation (Thirugnanaselvam, Gobi, and Arun Karthick 2013). In literature, it has been hypothesized that degradation of the soy protein-based scaffold leads to the release of some type of cryptic peptides which might play an important role in enhancing the healing process (Har-el et al. 2014).

2.5 Summary

We have demonstrated the method of fabrication of novel SPI/SF protein blend based nanofibers in various formulations. The morphological analysis of all the fabricated nanofibrous scaffolds using SEM micrographs accounts for the diameter of nanofibers in the range of 30 to 360 nm. Water retention assay depicted that SPI adds hydrophilicity and water retention ability to the SPI/SF scaffolds. Degradation study showed that we could modulate the degradability of nanofibers by changing the polymer ratio as per the

requirement. FTIR data and Raman spectral analysis revealed that EtOH vapor treatment induced the conversion of random coil structure to β sheet structure; providing stability to nanofibers which was also verified by the degradation analysis. EtOH vapor treatment to the nanofibers provides enhanced stability to the scaffold but at the cost of transparency. The cellular biocompatibility of the nanofibrous scaffold towards mammalian cells was investigated by MTT assay. Cell attachment and proliferation were qualitatively examined through SEM and fluorescent microscopic analysis. Cell culture studies revealed a noticeable increase in the extent of cellular growth correspondingly with a rise in the SPI content of scaffold. However, SPI concentration does not significantly influence the morphology of cells. Therefore, we anticipate that with all these properties, the prepared SPI/SF blend electrospun nanofibers could be an attractive material for many TE applications, especially for accelerating wound healing. In vivo wound healing in rats demonstrated the applicability of the SPI/SF nanofibers as a potential wound dressing material.

2.6 References

Ahmad, Zubair, K. Dinesh Kumar, Madhumita Saroop, Nisha Preschilla, Amit Biswas, Jayesh R. Bellare, and Anil K. Bhowmick. 2010. "Highly Transparent Thermoplastic Elastomer from Isotactic Polypropylene and Styrene/Ethylene-Butylene/Styrene Triblock Copolymer: Structure-Property Correlations." *Polymer Engineering & Science* 50 (2): 331–41. https://doi.org/10.1002/pen.21540.

Alessandrino, A., B. Marelli, C. Arosio, S. Fare, M. C. Tanzi, and G. Freddi. 2008. "Electrospun Silk Fibroin Mats for Tissue Engineering." *Engineering in Life Sciences* 8 (3): 219–25. https://doi.org/10.1002/elsc.200700067.

Bandyopadhyay, Ashutosh, Vimal Kumar Dewangan, Kiran Yellappa Vajanthri, Suruchi Poddar, and Sanjeev Kumar Mahto. 2018. "Easy and Affordable Method for Rapid Prototyping of Tissue Models in Vitro Using Three-Dimensional Bioprinting." *Biocybernetics and Biomedical Engineering* 38 (1): 158–69. https://doi.org/10.1016/j.bbe.2017.12.001.

Barhoum, Ahmed, Kaushik Pal, Hubert Rahier, Hasan Uludag, Ick Soo Kim, and Mikhael Bechelany. 2019. "Nanofibers as New-Generation Materials: From Spinning and Nano-Spinning Fabrication Techniques to Emerging Applications." *Applied Materials Today* 17 (December): 1–35. https://doi.org/10.1016/j.apmt.2019.06.015.

Bhardwaj, Nandana, and Subhas C. Kundu. 2010a. "Electrospinning: A Fascinating Fiber Fabrication Technique." *Biotechnology Advances* 28 (3): 325–47. https://doi.org/10.1016/j.biotechadv.2010.01.004.

Bhardwaj, N. and Kundu, S.C. 2010b. "Electrospinning: A Fascinating Fiber Fabrication Technique." *Biotechnology Advances* 28 (3): 325–47. https://doi.org/10.1016/j.biotechadv.2010.01.004.

Bonfield, William. 2006. "Designing Porous Scaffolds for Tissue Engineering." *Philosophical Transactions of the Royal Society A: Mathematical, Physical and Engineering Sciences* 364 (1838): 227–32. https://doi.org/10.1098/rsta.2005.1692.

Carrasco-Torres, Gabriela, Manuel A. Valdés-Madrigal, Verónica R. Vásquez-Garzón, Rafael Baltiérrez-Hoyos, Eduard De la Cruz-Burelo, Ramón Román-Doval, and Anaí A. Valencia-Lazcano. 2019. "Effect of Silk Fibroin on Cell Viability in Electrospun

Scaffolds of Polyethylene Oxide." *Polymers* 11 (3). https://doi.org/10.3390/polym11030451.

Catto, Valentina, Silvia Farè, Irene Cattaneo, Marina Figliuzzi, Antonio Alessandrino, Giuliano Freddi, Andrea Remuzzi, and Maria Cristina Tanzi. 2015. "Small Diameter Electrospun Silk Fibroin Vascular Grafts: Mechanical Properties, in Vitro Biodegradability, and in Vivo Biocompatibility." *Materials Science & Engineering. C, Materials for Biological Applications* 54 (September): 101–11. https://doi.org/10.1016/j.msec.2015.05.003.

Chatterjee, Cynthia, Stephen Gleddie, and Chao-Wu Xiao. 2018. "Soybean Bioactive Peptides and Their Functional Properties." *Nutrients* 10 (9). https://doi.org/10.3390/nu10091211.

Chen, Feng, and Jinwen Zhang. 2009. "A New Approach for Morphology Control of Poly(Butylene Adipate-Co-Terephthalate) and Soy Protein Blends." *Polymer* 50 (15): 3770–77. https://doi.org/10.1016/j.polymer.2009.06.004.

Chen, Honglin, Jin Huang, Jiahui Yu, Shiyuan Liu, and Ping Gu. 2011. "Electrospun Chitosan-Graft-Poly (ε -Caprolactone)/Poly (ε-Caprolactone) Cationic Nanofibrous Mats as Potential Scaffolds for Skin Tissue Engineering." *International Journal of Biological Macromolecules* 48 (1): 13–19. https://doi.org/10.1016/j.ijbiomac.2010.09.019.

Chen, Jyh-Ping, Shih-Hsien Chen, and Guo-Jyun Lai. 2012. "Preparation and Characterization of Biomimetic Silk Fibroin/Chitosan Composite Nanofibers by Electrospinning for Osteoblasts Culture." *Nanoscale Research Letters* 7 (1): 170. https://doi.org/10.1186/1556-276X-7-170.

Chien, Karen B., Brian A. Aguado, Paul J. Bryce, and Ramille N. Shah. 2013. "In Vivo Acute and Humoral Response to Three-Dimensional Porous Soy Protein Scaffolds." *Acta Biomaterialia* 9 (11): 8983–90. https://doi.org/10.1016/j.actbio.2013.07.005.

Cho, Daehwan, Anil N. Netravali, and Yong Lak Joo. 2012. "Mechanical Properties and Biodegradability of Electrospun Soy Protein Isolate/PVA Hybrid Nanofibers." *Polymer Degradation and Stability* 97 (5): 747–54. https://doi.org/10.1016/j.polymdegradstab.2012.02.007.

Dadras Chomachayi, Masoud, Atefeh Solouk, Somaye Akbari, Davoud Sadeghi, Fereshteh Mirahmadi, and Hamid Mirzadeh. 2018. "Electrospun Nanofibers Comprising

of Silk Fibroin/Gelatin for Drug Delivery Applications: Thyme Essential Oil and Doxycycline Monohydrate Release Study." *Journal of Biomedical Materials Research. Part A* 106 (4): 1092–1103. https://doi.org/10.1002/jbm.a.36303.

De Santis, Felice, and Roberto Pantani. 2013. "Optical Properties of Polypropylene upon Recycling." Research Article. The Scientific World Journal. 2013. https://doi.org/10.1155/2013/354093.

DeFrates, Kelsey G., Robert Moore, Julia Borgesi, Guowei Lin, Thomas Mulderig, Vince Beachley, and Xiao Hu. 2018. "Protein-Based Fiber Materials in Medicine: A Review." *Nanomaterials* 8 (7). https://doi.org/10.3390/nano8070457.

Eltom, Abdalla, Gaoyan Zhong, and Ameen Muhammad. 2019. "Scaffold Techniques and Designs in Tissue Engineering Functions and Purposes: A Review." Review Article. Advances in Materials Science and Engineering. 2019. https://doi.org/10.1155/2019/3429527.

Fan, Linpeng, Hongsheng Wang, Kuihua Zhang, Chuanglong He, Zengxiao Cai, and Xiumei Mo. 2012. "Regenerated Silk Fibroin Nanofibrous Matrices Treated with 75% Ethanol Vapor for Tissue-Engineering Applications." *Journal of Biomaterials Science. Polymer Edition* 23 (1–4): 497–508. https://doi.org/10.1163/092050610X552771.

Galvez, A. F., N. Chen, J. Macasieb, and B. O. de Lumen. 2001. "Chemopreventive Property of a Soybean Peptide (Lunasin) That Binds to Deacetylated Histones and Inhibits Acetylation." *Cancer Research* 61 (20): 7473–78.

Gonzalez de Mejia, Elvira, Miguel Vásconez, Ben O. de Lumen, and Randall Nelson. 2004. "Lunasin Concentration in Different Soybean Genotypes, Commercial Soy Protein, and Isoflavone Products." *Journal of Agricultural and Food Chemistry* 52 (19): 5882–87. https://doi.org/10.1021/jf0496752.

Har-el, Yah-el, Jonathan A. Gerstenhaber, Ross Brodsky, Richard B. Huneke, and Peter I. Lelkes. 2014. "Electrospun Soy Protein Scaffolds as Wound Dressings: Enhanced Reepithelialization in a Porcine Model of Wound Healing." *Wound Medicine* 5 (June): 9–15. https://doi.org/10.1016/j.wndm.2014.04.007.

Hu, Yongpei, Qin Zhang, Renchuan You, Lingshuang Wang, and Mingzhong Li. 2012. "The Relationship between Secondary Structure and Biodegradation Behavior of Silk

Fibroin Scaffolds." Research Article. Advances in Materials Science and Engineering. 2012. https://doi.org/10.1155/2012/185905.

Huang, Xiangyu, Suna Fan, Alhadi Ibrahim Mohammed Altayp, Yaopeng Zhang, Huili Shao, Xuechao Hu, Minkai Xie, and Yuemin Xu. 2014. "Tunable Structures and Properties of Electrospun Regenerated Silk Fibroin Mats Annealed in Water Vapor at Different Times and Temperatures." Research Article. Journal of Nanomaterials. 2014. https://doi.org/10.1155/2014/682563.

Jao, Dave, Ye Xue, Jethro Medina, and Xiao Hu. 2017. "Protein-Based Drug-Delivery Materials." *Materials* 10 (5). https://doi.org/10.3390/ma10050517.

Jeong, Hyung Jin, Jin Boo Jeong, Dae Seop Kim, and Ben O. de Lumen. 2007. "Inhibition of Core Histone Acetylation by the Cancer Preventive Peptide Lunasin." *Journal of Agricultural and Food Chemistry* 55 (3): 632–37. https://doi.org/10.1021/jf062405u.

Jiang, L. -B., D. -H. Su, P. Liu, Y. -Q. Ma, Z. -Z. Shao, and J. Dong. 2018. "Shape-Memory Collagen Scaffold for Enhanced Cartilage Regeneration: Native Collagen versus Denatured Collagen." *Osteoarthritis and Cartilage* 26 (10): 1389–99. https://doi.org/10.1016/j.joca.2018.06.004.

Jones, Vanessa, Joseph E Grey, and Keith G Harding. 2006. "Wound Dressings." *BMJ : British Medical Journal* 332 (7544): 777–80.

Khatib, K. A., T. J. Herald, F. M. Aramouni, F. MacRitchie, and W. T. Schapaugh. 2002. "Characterization and Functional Properties of Soy β-Conglycinin and Glycinin of Selected Genotypes." *Journal of Food Science* 67 (8): 2923–29. https://doi.org/10.1111/j.1365-2621.2002.tb08839.x.

Kim, So Hyun, Young Sik Nam, Taek Seung Lee, and Won Ho Park. 2003. "Silk Fibroin Nanofiber. Electrospinning, Properties, and Structure." *Polymer Journal* 35 (2): 185–90. https://doi.org/10.1295/polymj.35.185.

Lam, Yi, Alfredo Galvez, and Ben O. de Lumen. 2003. "Lunasin Suppresses E1A-Mediated Transformation of Mammalian Cells but Does Not Inhibit Growth of Immortalized and Established Cancer Cell Lines." *Nutrition and Cancer* 47 (1): 88–94. https://doi.org/10.1207/s15327914nc4701_11.

Lawrence, Brian D., Scott Wharram, Jonathan A. Kluge, Gary G. Leisk, Fiorenzo G. Omenetto, Mark I. Rosenblatt, and David L. Kaplan. 2010. “Effect of Hydration on Silk Film Material Properties.” *Macromolecular Bioscience* 10 (4): 393–403. https://doi.org/10.1002/mabi.200900294.

Li, Kaichang, Svetlana Peshkova, and Xinglian Geng. 2004. “Investigation of Soy Protein-Kymene® Adhesive Systems for Wood Composites.” *Journal of the American Oil Chemists’ Society* 81 (5): 487–91. https://doi.org/10.1007/s11746-004-0928-1.

Liu, Zhi, Feng Zhang, Jinfa Ming, Shiyu Bie, Junjuan Li, and Baoqi Zuo. 2015. “Preparation of Electrospun Silk Fibroin Nanofibers from Solutions Containing Native Silk Fibrils.” *Journal of Applied Polymer Science* 132 (1). https://doi.org/10.1002/app.41236.

Lu, Tingli, Yuhui Li, and Tao Chen. 2013. “Techniques for Fabrication and Construction of Three-Dimensional Scaffolds for Tissue Engineering.” *International Journal of Nanomedicine* 8: 337–50. https://doi.org/10.2147/IJN.S38635.

Lubasova, Daniela, Jana Mullerova, and Anil N. Netravali. 2015. “Water-Resistant Plant Protein-Based Nanofiber Membranes.” *Journal of Applied Polymer Science* 132 (16). https://doi.org/10.1002/app.41852.

Lule, Vaibhao Kisanrao, Sheenam Garg, Sarang Dilip Pophaly, null Hitesh, and Sudhir Kumar Tomar. 2015. “Potential Health Benefits of Lunasin: A Multifaceted Soy-Derived Bioactive Peptide.” *Journal of Food Science* 80 (3): R485-494. https://doi.org/10.1111/1750-3841.12786.

MacKay, Douglas, and Alan L. Miller. 2003. “Nutritional Support for Wound Healing.” *Alternative Medicine Review: A Journal of Clinical Therapeutic* 8 (4): 359–77.

Marcolin, Chiara, Lorenza Draghi, MariaCristina Tanzi, and Silvia Faré. 2017. “Electrospun Silk Fibroin-Gelatin Composite Tubular Matrices as Scaffolds for Small Diameter Blood Vessel Regeneration.” *Journal of Materials Science. Materials in Medicine* 28 (5): 80. https://doi.org/10.1007/s10856-017-5884-9.

Marelli, Benedetto, Matteo Achilli, Antonio Alessandrino, Giuliano Freddi, Maria Cristina Tanzi, Silvia Farè, and Diego Mantovani. 2012. “Collagen-Reinforced Electrospun Silk Fibroin Tubular Construct as Small Calibre Vascular Graft.” *Macromolecular Bioscience* 12 (11): 1566–74. https://doi.org/10.1002/mabi.201200195.

Mejia, Elvira De, and Ben O. De Lumen. 2006. “Soybean Bioactive Peptides: A New Horizon in Preventing Chronic Diseases.” *Sexuality, Reproduction and Menopause* 4 (2): 91–95. https://doi.org/10.1016/j.sram.2006.08.012.

Merolli, Antonio, Luigi Nicolais, Luigi Ambrosio, and Matteo Santin. 2010. “A Degradable Soybean-Based Biomaterial Used Effectively as a Bone Fillerin Vivoin a Rabbit.” *Biomedical Materials* 5 (1): 015008. https://doi.org/10.1088/1748-6041/5/1/015008.

Mogoşanu, George Dan, and Alexandru Mihai Grumezescu. 2014. “Natural and Synthetic Polymers for Wounds and Burns Dressing.” *International Journal of Pharmaceutics*, Improved Wound Dressing: Novel Approaches, 463 (2): 127–36. https://doi.org/10.1016/j.ijpharm.2013.12.015.

Nagarajan, Sakthivel, Habib Belaid, Céline Pochat-Bohatier, Catherine Teyssier, Igor Iatsunskyi, Emerson Coy, Sébastien Balme, et al. 2017. “Design of Boron Nitride/Gelatin Electrospun Nanofibers for Bone Tissue Engineering.” *ACS Applied Materials & Interfaces* 9 (39): 33695–706. https://doi.org/10.1021/acsami.7b13199.

Nicholas, Mathew N., Marc G. Jeschke, and Saeid Amini-Nik. 2016. “Methodologies in Creating Skin Substitutes.” *Cellular and Molecular Life Sciences: CMLS* 73 (18): 3453–72. https://doi.org/10.1007/s00018-016-2252-8.

Ning, Wane, Jiwei Huang, Xinlong Ling, and Haitao Lin. 2018. “Modification of Electrospun Silk Fibroin Nanofiber Mats: Using an EDC/NHS Ethanol Solvent.” *IOP Conference Series: Materials Science and Engineering* 423 (November): 012068. https://doi.org/10.1088/1757-899X/423/1/012068.

Olami, H, I Berdicevsky, and M Zilberman. 2015. “Novel Soy Protein Blend Scaffolds Loaded with Antibiotics: Drug Release Profile—Bacterial Inhibition Effects,” 9.

Pabona, John Mark P., Bhuvanesh Dave, Ying Su, Maria Theresa E. Montales, Ben O. de Lumen, Elvira G. de Mejia, Omar M. Rahal, and Rosalia C. M. Simmen. 2013. “The Soybean Peptide Lunasin Promotes Apoptosis of Mammary Epithelial Cells via Induction of Tumor Suppressor PTEN: Similarities and Distinct Actions from Soy Isoflavone Genistein.” *Genes & Nutrition* 8 (1): 79–90. https://doi.org/10.1007/s12263-012-0307-5.

Park, Ko Eun, Sung Youn Jung, Seung Jin Lee, Byung-Moo Min, and Won Ho Park. 2006. “Biomimetic Nanofibrous Scaffolds: Preparation and Characterization of

Chitin/Silk Fibroin Blend Nanofibers." *International Journal of Biological Macromolecules* 38 (3–5): 165–73. https://doi.org/10.1016/j.ijbiomac.2006.03.003.

Peles, Zachi, and Meital Zilberman. 2012. "Novel Soy Protein Wound Dressings with Controlled Antibiotic Release: Mechanical and Physical Properties." *Acta Biomaterialia* 8 (1): 209–17. https://doi.org/10.1016/j.actbio.2011.08.022.

Phiriyawirut, M., N. Rodchanacheewa, N. Nensiri, and Pitt Supaphol. 2008. "Morphology of Electrospun Mats of Soy Protein Isolate and Its Blend." Advanced Materials Research. 2008. https://doi.org/10.4028/www.scientific.net/AMR.55-57.733.

Poddar, Suruchi, Piyush Sunil Agarwal, Ajay Kumar Sahi, Kiran Yellappa Vajanthri, Pallawi, K. N. Singh, and Sanjeev Kumar Mahto. 2019. "Fabrication and Cytocompatibility Evaluation of Psyllium Husk (Isabgol)/Gelatin Composite Scaffolds." *Applied Biochemistry and Biotechnology* 188 (3): 750–68. https://doi.org/10.1007/s12010-019-02958-7.

Ramji, Karpagavalli, and Ramille N. Shah. 2014. "Electrospun Soy Protein Nanofiber Scaffolds for Tissue Regeneration." *Journal of Biomaterials Applications* 29 (3): 411–22. https://doi.org/10.1177/0885328214530765.

Ren, Dongwen, Hongfu Yi, Wei Wang, and Xiaojun Ma. 2005. "The Enzymatic Degradation and Swelling Properties of Chitosan Matrices with Different Degrees of N-Acetylation." *Carbohydrate Research* 340 (15): 2403–10. https://doi.org/10.1016/j.carres.2005.07.022.

Rockwood, Danielle N., Rucsanda C. Preda, Tuna Yücel, Xiaoqin Wang, Michael L. Lovett, and David L. Kaplan. 2011. "Materials Fabrication from Bombyx Mori Silk Fibroin." *Nature Protocols* 6 (10). https://doi.org/10.1038/nprot.2011.379.

Salas, Carlos, Mariko Ago, Lucian A. Lucia, and Orlando J. Rojas. 2014. "Synthesis of Soy Protein–Lignin Nanofibers by Solution Electrospinning." *Reactive and Functional Polymers* 85 (December): 221–27. https://doi.org/10.1016/j.reactfunctpolym.2014.09.022.

Santin, Matteo, and Luigi Ambrosio. 2008. "Soybean-Based Biomaterials: Preparation, Properties and Tissue Regeneration Potential." *Expert Review of Medical Devices* 5 (3): 349–58. https://doi.org/10.1586/17434440.5.3.349.

Santin, Matteo, Christopher Morris, Guy Standen, Luigi Nicolais, and Luigi Ambrosio. 2007. “A New Class of Bioactive and Biodegradable Soybean-Based Bone Fillers.” *Biomacromolecules* 8 (9): 2706–11. https://doi.org/10.1021/bm0703362.

Schneider, A., X. Y. Wang, D. L. Kaplan, J. A. Garlick, and C. Egles. 2009. “Biofunctionalized Electrospun Silk Mats as a Topical Bioactive Dressing for Accelerated Wound Healing.” *Acta Biomaterialia* 5 (7): 2570–78. https://doi.org/10.1016/j.actbio.2008.12.013.

Shahverdi, Sheida, Mirhamed Hajimiri, Mohammad Amin Esfandiari, Bagher Larijani, Fatemeh Atyabi, Afsaneh Rajabiani, Ahmad Reza Dehpour, Ali Akbar Gharehaghaji, and Rassoul Dinarvand. 2014. “Fabrication and Structure Analysis of Poly(Lactide-Co-Glycolic Acid)/Silk Fibroin Hybrid Scaffold for Wound Dressing Applications.” *International Journal of Pharmaceutics* 473 (1–2): 345–55. https://doi.org/10.1016/j.ijpharm.2014.07.021.

Shidal, Chris, Jun-Ichi Inaba, Kavitha Yaddanapudi, and Keith R. Davis. 2017. “The Soy-Derived Peptide Lunasin Inhibits Invasive Potential of Melanoma Initiating Cells.” *Oncotarget* 8 (15): 25525–41. https://doi.org/10.18632/oncotarget.16066.

Silva, G. A., C. M. Vaz, O. P. Coutinho, A. M. Cunha, and R. L. Reis. 2003. “In Vitro Degradation and Cytocompatibility Evaluation of Novel Soy and Sodium Caseinate-Based Membrane Biomaterials.” *Journal of Materials Science. Materials in Medicine* 14 (12): 1055–66. https://doi.org/10.1023/b:jmsm.0000004002.11278.30.

Silva, Raquel, Buse Bulut, Judith A. Roether, Joachim Kaschta, Dirk W. Schubert, and Aldo R. Boccaccini. 2014. “Sonochemical Processing and Characterization of Composite Materials Based on Soy Protein and Alginate Containing Micron-Sized Bioactive Glass Particles.” *Journal of Molecular Structure* Complete (1073): 87–96. https://doi.org/10.1016/j.molstruc.2014.05.047.

Singh, Brij Pal, Shilpa Vij, and Subrota Hati. 2014. “Functional Significance of Bioactive Peptides Derived from Soybean.” *Peptides* 54 (April): 171–79. https://doi.org/10.1016/j.peptides.2014.01.022.

Tansaz, Samira, Liliana Liverani, Lars Vester, and Aldo R. Boccaccini. 2017. “Soy Protein Meets Bioactive Glass: Electrospun Composite Fibers for Tissue Engineering

Applications." *Materials Letters* 199 (July): 143–46. https://doi.org/10.1016/j.matlet.2017.04.042.

Tansaz, Samira, Raminder Singh, Iwona Cicha, and Aldo R. Boccaccini. 2018. "Soy Protein-Based Composite Hydrogels: Physico-Chemical Characterization and In Vitro Cytocompatibility." *Polymers* 10 (10). https://doi.org/10.3390/polym10101159.

Thenmozhi, S., N. Dharmaraj, K. Kadirvelu, and Hak Yong Kim. 2017. "Electrospun Nanofibers: New Generation Materials for Advanced Applications." *Materials Science and Engineering: B* 217 (March): 36–48. https://doi.org/10.1016/j.mseb.2017.01.001.

Thirugnanaselvam, M., N. Gobi, and S. Arun Karthick. 2013. "SPI/PEO Blended Electrospun Martrix for Wound Healing." *Fibers and Polymers* 14 (6): 965–69. https://doi.org/10.1007/s12221-013-0965-y.

Tian, Huafeng, Guozhi Xu, Biao Yang, and Gaiping Guo. 2011. "Microstructure and Mechanical Properties of Soy Protein/Agar Blend Films: Effect of Composition and Processing Methods." *Journal of Food Engineering* 107 (1): 21–26. https://doi.org/10.1016/j.jfoodeng.2011.06.008.

Varshney, Neelima, Ajay Kumar Sahi, Kiran Yellappa Vajanthri, Suruchi Poddar, Chelladurai Karthikeyan Balavigneswaran, Arumugam Prabhakar, Vivek Rao, and Sanjeev Kumar Mahto. 2019. "Culturing Melanocytes and Fibroblasts within Three-Dimensional Macroporous PDMS Scaffolds: Towards Skin Dressing Material." *Cytotechnology* 71 (1): 287–303. https://doi.org/10.1007/s10616-018-0285-6.

Vasconcelos, Andreia, Andreia C. Gomes, and Artur Cavaco-Paulo. 2012. "Novel Silk Fibroin/Elastin Wound Dressings." *Acta Biomaterialia* 8 (8): 3049–60. https://doi.org/10.1016/j.actbio.2012.04.035.

Vu Huu Thanh and Kazuo Shibasaki. 1977. "Beta-Conglycinin from Soybean Proteins. Isolation and Immunological and Physicochemical Properties of the Monomeric Forms." *Biochimica et Biophysica Acta (BBA) - Protein Structure* 490 (2): 370–84. https://doi.org/10.1016/0005-2795(77)90012-5.

Wang, Wenyi, Vermont P. Dia, Miguel Vasconez, Elvira Gonzalez de Mejia, and Randall L. Nelson. 2008. "Analysis of Soybean Protein-Derived Peptides and the Effect of Cultivar, Environmental Conditions, and Processing on Lunasin Concentration in Soybean and Soy Products." *Journal of AOAC International* 91 (4): 936–46.

Wang, Yi-Chieh, Roch-Chui Yu, and Cheng-Chun Chou. 2006. “Antioxidative Activities of Soymilk Fermented with Lactic Acid Bacteria and Bifidobacteria.” *Food Microbiology* 23 (2): 128–35. https://doi.org/10.1016/j.fm.2005.01.020.

Wang, Yixiang, Xiaodong Cao, and Lina Zhang. 2006. “Effects of Cellulose Whiskers on Properties of Soy Protein Thermoplastics.” *Macromolecular Bioscience* 6 (7): 524–31. https://doi.org/10.1002/mabi.200600034.

Xu, Xuezhu, Long Jiang, Zhengping Zhou, Xiangfa Wu, and Yechun Wang. 2012. “Preparation and Properties of Electrospun Soy Protein Isolate/Polyethylene Oxide Nanofiber Membranes.” *ACS Applied Materials & Interfaces* 4 (8): 4331–37. https://doi.org/10.1021/am300991e.

Ye, Kaiqiang, Haizhu Kuang, Zhengwei You, Yosry Morsi, and Xiumei Mo. 2019. “Electrospun Nanofibers for Tissue Engineering with Drug Loading and Release.” *Pharmaceutics* 11 (4). https://doi.org/10.3390/pharmaceutics11040182.

Yin-Guibo, Zhang-Youzhu, Bao-Weiwei, Wu-Jialin, Shi De-bing, Dong Zhi-hui, and Fu Wei-guo. 2009. “Study on the Properties of the Electrospun Silk Fibroin/Gelatin Blend Nanofibers for Scaffolds.” *Journal of Applied Polymer Science* 111 (3): 1471–77. https://doi.org/10.1002/app.28963.

Yoo, Choung Ryong, In-Sung Yeo, Ko Eun Park, Ji Hun Park, Seung Jin Lee, Won Ho Park, and Byung-Moo Min. 2008. “Effect of Chitin/Silk Fibroin Nanofibrous Bicomponent Structures on Interaction with Human Epidermal Keratinocytes.” *International Journal of Biological Macromolecules* 42 (4): 324–34. https://doi.org/10.1016/j.ijbiomac.2007.12.004.

Yoshie-Stark, Yumiko, Yoshiko Wada, and Andreas Wäsche. 2008. “Chemical Composition, Functional Properties, and Bioactivities of Rapeseed Protein Isolates.” *Food Chemistry* 107 (1): 32–39. https://doi.org/10.1016/j.foodchem.2007.07.061.

Zhang, Feng, Jian N. Wang, and Bao Q. Zuo. 2010. “Effect of Aqueous Ethanol Treatment on the Electrospun SF Nanofiber Mats.” In *2010 4th International Conference on Bioinformatics and Biomedical Engineering*, 1–4. https://doi.org/10.1109/ICBBE.2010.5515644.

Zhang, Jinwen, Long Jiang, Linyong Zhu, Jay-lin Jane, and Perminus Mungara. 2006. "Morphology and Properties of Soy Protein and Polylactide Blends." *Biomacromolecules* 7 (5): 1551–61. https://doi.org/10.1021/bm050888p.